Magnetized stratified rotating shear waves

Abdelaziz Salhi, Thierry Lehner, Fabien S. Godeferd, Claude Cambon

Magnetized stratified rotating shear waves

A. Salhi,[1] T. Lehner,[2] F. Godeferd,[3] and C. Cambon[3]
[1]*Département de Physique, Faculté des Sciences de Tunis, 1060 Tunis, Tunisia*
[2]*LUTH, Observatoire de Paris-Meudon, 5 place de Janssen, 92195 Meudon*
[3]*Laboratoire de Mécanique des Fluides et d' Acoustique, Ecole Centrale de Lyon, UMR 5509, CNRS, INSA, UCB, 69134 Ecully Cedex, France*
(Received 27 June 2011; published 1 February 2012)

We present a spectral linear analysis in terms of advected Fourier modes to describe the behavior of a fluid submitted to four constraints: shear (with rate S), rotation (with angular velocity Ω), stratification, and magnetic field within the linear spectral theory or the shearing box model in astrophysics. As a consequence of the fact that the base flow must be a solution of the Euler-Boussinesq equations, only radial and/or vertical density gradients can be taken into account. Ertel's theorem no longer is valid to show the conservation of potential vorticity, in the presence of the Lorentz force, but a similar theorem can be applied to a potential magnetic induction: The scalar product of the density gradient by the magnetic field is a Lagrangian invariant for an inviscid and nondiffusive fluid. The linear system with a minimal number of solenoidal components, two for both velocity and magnetic disturbance fields, is eventually expressed as a four-component inhomogeneous linear differential system in which the buoyancy scalar is a combination of solenoidal components (variables) and the (constant) potential magnetic induction. We study the stability of such a system for both an infinite streamwise wavelength ($k_1 = 0$, axisymmetric disturbances) and a finite one ($k_1 \neq 0$, nonaxisymmetric disturbances). In the former case ($k_1 = 0$), we recover and extend previous results characterizing the magnetorotational instability (MRI) for combined effects of radial and vertical magnetic fields and combined effects of radial and vertical density gradients. We derive an expression for the MRI growth rate in terms of the stratification strength, which indicates that purely radial stratification can inhibit the MRI instability, while purely vertical stratification cannot completely suppress the MRI instability. In the case of nonaxisymmetric disturbances ($k_1 \neq 0$), we only consider the effect of vertical stratification, and we use Levinson's theorem to demonstrate the stability of the solution at infinite vertical wavelength ($k_3 = 0$): There is an oscillatory behavior for $\tau > 1 + |K_2/k_1|$, where $\tau = St$ is a dimensionless time and K_2 is the radial component of the wave vector at $\tau = 0$. The model is suitable to describe instabilities leading to turbulence by the bypass mechanism that can be relevant for the analysis of magnetized stratified Keplerian disks with a purely azimuthal field. For initial isotropic conditions, the time evolution of the spectral density of total energy (kinetic + magnetic + potential) is considered. At $k_3 = 0$, the vertical motion is purely oscillatory, and the sum of the vertical (kinetic + magnetic) energy plus the potential energy does not evolve with time and remains equal to its initial value. The horizontal motion can induce a rapid transient growth provided $K_2/k_1 \gg 1$. This rapid growth is due to the aperiodic velocity vortex mode that behaves like K_h/k_h where $k_h(\tau) = [k_1^2 + (K_2 - k_1\tau)^2]^{1/2}$ and $K_h = k_h(0)$. After the leading phase ($\tau > K_2/k_1 \gg 1$), the horizontal magnetic energy and the horizontal kinetic energy exhibit a similar (oscillatory) behavior yielding a high level of total energy. The contribution to energies coming from the modes $k_1 = 0$ and $k_3 = 0$ is addressed by investigating the one-dimensional spectra for an initial Gaussian dense spectrum. For a magnetized Keplerian disk with a purely vertical field, it is found that an important contribution to magnetic and kinetic energies comes from the region near $k_1 = 0$. The limit at $k_1 = 0$ of the streamwise one-dimensional spectra of energies, or equivalently, the streamwise two-dimensional (2D) energy, is then computed. The comparison of the ratios of these 2D quantities with their three-dimensional counterparts provided by previous direct numerical simulations shows a quantitative agreement.

DOI: 10.1103/PhysRevE.85.026301 PACS number(s): 47.27.W−, 47.20.Cq, 47.27.Cn, 97.10.Gz

I. INTRODUCTION

An enormous amount of literature is devoted to the stability of accretion disks and their turbulent regime (see, e.g., Refs. [1–6]). Among these papers, a very productive approach is based on the shearing sheet formalism (see Refs. [2,7–10]). The related model for the base or mean flow is a pure plane shear flow, with uniform shear rate S, seen in a rotating frame with angular velocity Ω in the spanwise (normal to the plane of the shear) direction. This basic flow in Cartesian coordinates (x_1, x_2, and x_3, for streamwise, cross-gradient, and spanwise mean-shear directions here, see Fig. 1) corresponds to the limit of a Taylor-Couette flow with differential rotation $\tilde{\Omega}(r) \sim r^{-q}$ in the radial direction so that $S = -r\partial\tilde{\Omega}/\partial r \sim -qr^{-q}$, at a given r, and streamwise, cross-gradient, and spanwise, directions in Cartesian coordinates correspond to peripheral, radial, and axial directions in cylindrical coordinates.

The development of disturbances to this base flow was studied in different communities, engineering, applied mathematics, and geophysics. Common tools, shared with astrophysicists and rediscussed below, are spectral linear theory, referred to as SLT hereinafter, and nonlinear pseudospectral direct numerical simulations (DNSs) in a frame comoving with the mean-shear flow [11,12].

Using a simplified pressureless analysis, it is shown that the Rayleigh criterion and engineering models give the same results: The stability is conditioned by the sign of the square of

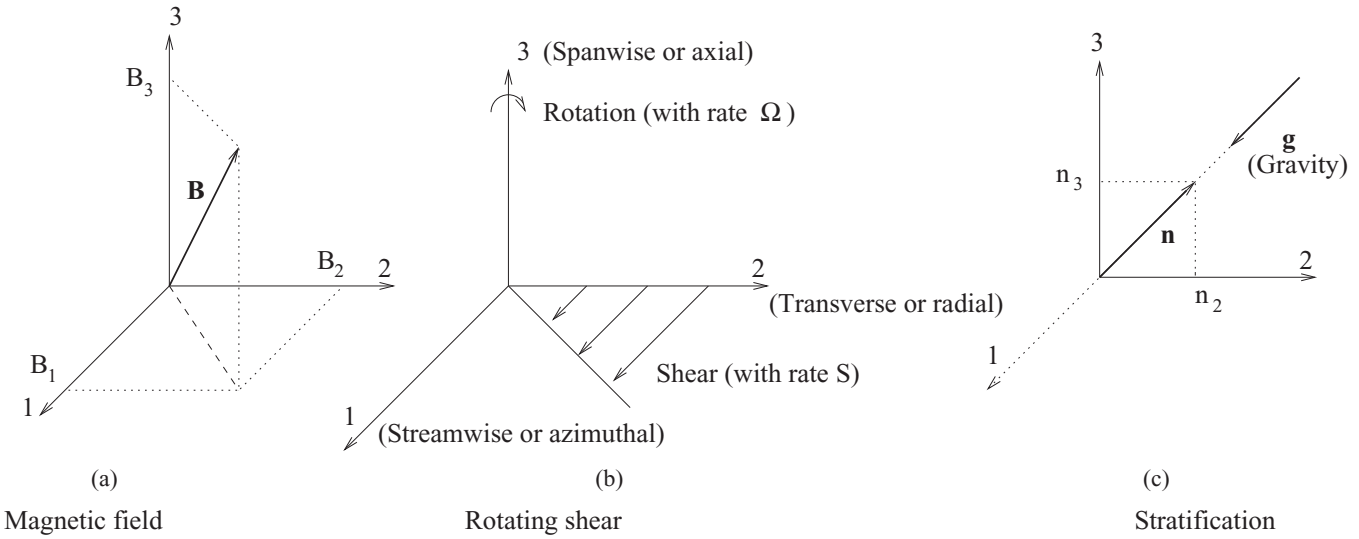

FIG. 1. Sketch of the unbounded rotating sheared flow.

the epicyclic frequency κ, which corresponds to the Bradshaw number or rotational Richardson number [13–15],

$$\kappa^2 = 2\Omega(2\Omega - S), \tag{1}$$

or equivalently, for anticyclonic rotation as in astrophysical disks,

$$\kappa^2 = 4\tilde{\Omega}^2 + \frac{d\tilde{\Omega}^2}{d\ \ln r} = 2(2-q)\tilde{\Omega}^2, \tag{2}$$

with exponential growth for $\kappa^2 < 0$ (i.e., $q > 2$) and stability for other cases (i.e., $0 < q \leqslant 2$). Note that the case of solid body rotation is characterized by $q = 0$. Accordingly, linear instability occurs for $-1 < R_\Omega \equiv -2\Omega/S < 0$. As a very important example, the Keplerian disk, with $\tilde{\Omega}(r) = r^{-q}$, $q = 3/2$, gives $R_\Omega = -4/3$ and, therefore, is considered as stable.

Even if complete SLT does not question these results, it is potentially much more powerful than the pressureless analysis, as we will show later with additional effects of stratification and magnetohydrodynamics (MHD). This approach, known as rapid distortion theory (RDT) from several authors in Cambridge (see, e.g., Refs. [16–19]), and rediscovered in applied mathematics, especially for the case of elliptical instability (see, e.g., Refs. [20–27]), used disturbances in terms of mean-flow-advected Fourier modes, with a time-dependent wave vector, called Kelvin modes, shear waves, spatial Fourier harmonics (SFH), see, e.g., Ref. [28]), depending on the community. Exact treatment of pressure fluctuation, for instance, is unavoidable for understanding the basic elliptical flow instability. In addition, exponential time dependency of mode amplitudes, which satisfy a linear system of ordinary differential equations (ODE), is not prescribed as in normal-mode analysis so that algebraic growth is permitted, with an implication in transient growth and mode coupling emphasized in, e.g., Ref. [29]. These authors even refer to SLT as a standard procedure of nonmodal analysis: Perhaps standard is questionable, because SLT, or RDT is not even mentioned in a recent review of nonmodal stability theory [30].

Faced with the evidence of the turbulent aspect of Keplerian disks, one has to take a more complex model for the disk than the rotating shear flow into account. Setting aside fully nonlinear stability analysis (see, e.g., Refs. [31,32]), nonlocal analysis with global flow curvature (see, e.g., Ref. [33]), significant compressibility (see, e.g., Ref. [34]), and confinement—except in Appendix C here—(see Ref. [35]) we will follow two angles of attack with the possibility to combine them.

The first one is to add density stratification. From this viewpoint, the studies in Refs. [36] and [29] are important, and our refined analysis (Salhi *et al.* [37]) is a followup. In addition, the latter paper can be seen as a first part of the present one as well, for rotating stratified nonmagnetized, disks. The main results in Ref. [37] can be gathered as follows: (i) A single dispersion relation is given for the axisymmetric mode $k_1 = 0$, showing a possible destabilization of the rotating shear by mean stratification; (ii) stability is proven by the Levinson theorem, more suitable than Wentzel-Kramers-Brillouin (WKB), for $k_1 \neq 0$, but very promising effects of dramatic transient growth and mode coupling are found in the stable case, in connection with a generalized wave-vortex decomposition.

In this context, the stratification can be related to a baroclinic effect [38]. Klar (2004) [39] studied a transient convective baroclinic instability due to an entropy gradient. The analysis accounts for a differential rotation, which is corrected by the radial stratification, rendering $\tilde{\Omega}$ *sub-Keplerian*, i.e., smaller than its Keplerian value. In Klar and Bodenheimer (2003) [40], a radial negative entropy gradient is assessed in protoplanetary disks, and thermal convection is revisited. The context is baroclinic, again, with dependence on the angular velocity with respect to the radial density gradient. The simple model of density gradient for the base flow used in this paper cannot include a baroclinic effect. The density gradient remains aligned with the gravitational acceleration, and the baroclinic torque is zero. The local angular velocity is independent of the density gradient in our model as well. Strict incompressibility is assumed so that a study of interchanges and mode coupling including a dilatational mode, as in Tevzadze *et al.* (2010) [41], is not relevant.

The second one is to add MHD coupling, introducing a base (mean) magnetic field and considering the flow as electrically conducting. The magnetorotational instability (MRI) is very interesting in this context because it can affect the Keplerian disk (see Balbus and Hawley [2] for a review). MHD coupling is very important in our paper and not the baroclinic context for unmagnetized disks precedingly touched upon.

The accumulated experience on various approaches is used here to optimize the SLT analysis for rotating stratified magnetized shear flow along the following lines:

(1) Use of admissibility conditions. According to Ref. [22], this means that the mean flow is a particular solution of the Euler-Boussineq-induction equations as a base flow for stability analysis. This also is consistent with statistical homogeneity restricted to fluctuations, which suppresses the feedback from the Reynolds stress tensor(s) in the mean-flow equation(s), whereas, viscous terms are zero for a space-linear velocity, density, and magnetic mean fields.

(2) Identification of the basic Green's function, denoted **g** from now on, in terms of a minimal number of solenoidal modes. This method is applied systematically from Cambon's thesis (1982) with its first publication in English in Ref. [24]. The fluctuating velocity and magnetic (its potential vector here) fields are expressed in terms of two components, toroidal and poloidal, with exact removal of pressure, whereas, the buoyancy scalar is scaled as a velocity, with its variance directly related to the potential energy. The linear problem in terms of eight components (three velocity components, three magnetic components, one buoyancy scalar, one for pressure) is turned into a five-component one, and the basic Green's function reduces to a rank-5 one.

(3) Use of Ertel's theorem except if it is no longer valid in the presence of MHD.

In the presence of the induction equation, and especially because of the presence of the Lorentz force as its magnetic feedback in the momentum equation, Ertel's theorem used in nonmagnetized stratified disks no longer works. In counterpart, the analogy of the induction equation with the vorticity equation allows us to replace the potential vorticity, as a scalar product of vorticity by density gradient, by a potential magnetic induction, as the scalar product of the magnetic vector by the density gradient. A magnetic counterpart of the linearized potential vorticity, or Ertel invariant, therefore, is derived, allowing to reduce the rank of the linear system of equations from 5 to 4.

As in our preceding papers, the basic Green's function is not only used for analyzing the stability of single disturbance modes, but also for predicting typical second-order statistical quantities as well, such as one-dimensional energy spectra, related two-dimensional (2D) energy components and Reynolds stress components as in Refs. [15,42]. In this sense, our SLT analysis is not monomodal but simultaneously involves different modes, either from the viewpoint of coupling of modes or from the viewpoint of prediction of statistics from initial disturbances with a dense spectrum.

The paper is organized as follows. Basic Navier-Stokes-Boussinesq and induction equations are given in Sec. II, and the base flow is specified according to admissibility conditions. Linearized equations for SLT are given in Sec. II. They are solved and are discussed in Sec. IV for the axisymmetric case $k_1 = 0$, with extended analytical results for the MRI growth rate. Section V is devoted to the case $k_1 \neq 0$, using Levinson's theorem for proving stability, if needed. Transient growth, in the case with a purely azimuthal magnetic field, is addressed in Sec. VI with numerical results. Typical ratios of 2D energy components are given in Sec. VII with comparison with existing DNS results. Section VIII is devoted to the conclusion and perspectives.

II. MHD BOUSSINESQ EQUATIONS

A. Background equations

The fluid is assumed to be inviscid and nondiffusive. The validity of the Boussinesq approximations for a rotating stratified sheared flow in a magnetic field was addressed in the paper by Balbus and Hawley [43], and it will not be recalled here. Under the Boussinesq approximations, the equations describing the evolution of the velocity field $\tilde{\boldsymbol{u}}$, the magnetic field $\tilde{\boldsymbol{b}}$, and the buoyancy field $\tilde{\theta}$ are the Navier-Stokes equations with the Lorentz and Coriolis forces, the induction equation, and the equation for the buoyancy scalar,

$$\frac{\partial \tilde{\boldsymbol{u}}}{\partial t} + (\tilde{\boldsymbol{u}}\cdot\boldsymbol{\nabla})\tilde{\boldsymbol{u}} = -\boldsymbol{\nabla}\tilde{p} - 2\boldsymbol{\Omega}\times\tilde{\boldsymbol{u}} + \tilde{\theta}\boldsymbol{n} + \frac{1}{\rho_0\mu_0}(\boldsymbol{\nabla}\times\tilde{\boldsymbol{b}})\times\tilde{\boldsymbol{b}}, \tag{3}$$

$$\frac{\partial \tilde{\boldsymbol{b}}}{\partial t} + (\tilde{\boldsymbol{u}}\cdot\boldsymbol{\nabla})\tilde{\boldsymbol{b}} = (\tilde{\boldsymbol{b}}\cdot\boldsymbol{\nabla})\tilde{\boldsymbol{u}}, \tag{4}$$

$$(\partial_t + \tilde{\boldsymbol{u}}\cdot\boldsymbol{\nabla})\tilde{\theta} = 0, \tag{5}$$

$$\boldsymbol{\nabla}\cdot\tilde{\boldsymbol{u}} = 0, \qquad \boldsymbol{\nabla}\cdot\tilde{\boldsymbol{b}} = 0, \tag{6}$$

where $\tilde{p}$ is the pressure divided by a reference density ρ_0 and includes the centrifugal potential, $\boldsymbol{n} = (n_1, n_2, n_3)^T$ denotes the fixed unit vector antiparallel to the gravitational acceleration $\boldsymbol{g}$, and μ_0 is the magnetic permeability. The buoyancy term $\tilde{\theta}$ is proportional to the gravitational acceleration and to a density (for a liquid) or a potential temperature (for a gas) and even to a scalar concentration (salt). The displacement current in the Maxwell-Ampère equation is neglected so that $\boldsymbol{\nabla}\times\tilde{\boldsymbol{b}} = \mu_0\tilde{\boldsymbol{j}}$, where $\tilde{\boldsymbol{j}}$ is the density of the electric current.

B. The magnetic potential

The equation for the absolute vorticity $\tilde{\boldsymbol{\omega}} = \boldsymbol{\nabla}\tilde{\boldsymbol{u}} + 2\boldsymbol{\Omega}$ is obtained by applying the curl to Eq. (3) (see, e.g., Ref. [44]),

$$(\partial_t + \tilde{\boldsymbol{u}}\cdot\boldsymbol{\nabla})\tilde{\boldsymbol{\omega}} = (\tilde{\boldsymbol{\omega}}\cdot\boldsymbol{\nabla})\tilde{\boldsymbol{u}} + \boldsymbol{\nabla}\times(\tilde{\theta}\boldsymbol{n}) + \frac{1}{\rho_0}\boldsymbol{\nabla}\times(\tilde{\boldsymbol{j}}\times\tilde{\boldsymbol{b}}). \tag{7}$$

Due to the presence of the Lorentz force in the electrically conducting fluid so that the last term on the right hand side of Eq. (7) is not zero, the absolute potential vorticity $\pi = \tilde{\boldsymbol{\omega}}\cdot\boldsymbol{\nabla}\tilde{\theta}$ does not constitute a Lagrangian invariant,

$$(\partial_t + \tilde{\boldsymbol{u}}\cdot\boldsymbol{\nabla})\tilde{\pi} = \left[\frac{1}{\rho_0}\boldsymbol{\nabla}\times(\tilde{\boldsymbol{j}}\times\tilde{\boldsymbol{b}})\right]\cdot(\boldsymbol{\nabla}\tilde{\theta})$$

for an inviscid and nondiffusive fluid. It is, rather, the potential magnetic induction,

$$\tilde{\pi}_m = \tilde{\boldsymbol{b}}\cdot\boldsymbol{\nabla}\tilde{\theta} = (\boldsymbol{\nabla}\times\tilde{\boldsymbol{a}})\cdot\boldsymbol{\nabla}\tilde{\theta}, \tag{8}$$

which is a Lagrangian invariant, or

$$(\partial_t + \tilde{\boldsymbol{u}}\cdot\boldsymbol{\nabla})\tilde{\pi}_m = 0. \tag{9}$$

Here, $\tilde{\boldsymbol{a}}$ is the vector potential of the magnetic field, with $\tilde{\boldsymbol{b}} = \boldsymbol{\nabla}\times\tilde{\boldsymbol{a}}$, which satisfies Coulomb's gauge $\boldsymbol{\nabla}\cdot\tilde{\boldsymbol{a}} = 0$ since the displacement current is neglected.

C. Base flow

The base flow considered in the present paper consists of a horizontal plane shear in a frame rotating about the vertical axis (Fig. 1),

$$\boldsymbol{u} = \mathbf{A}\cdot\boldsymbol{x}, \quad A_{ij} = S\delta_{i1}\delta_{j2}, \quad \boldsymbol{\Omega} = (0,0,\Omega)^T, \tag{10}$$

where both the shear and the rotation rates are constant. The basic buoyancy scalar Θ varies linearly with the space coordinates,

$$\Theta = -\frac{\rho_0}{g}\left(N_1^2 x_1 + N_2^2 x_2 + N_3^2 x_3\right),$$

around the reference density ρ_0, where N_1^2, N_2^2, and N_3^2 are constants and represent the square of Brunt-Väsälä frequencies with respect to the (x_1,x_2,x_3) directions, respectively, and g is the gravity acceleration. The above base flow must be a solution of Eqs. (3)–(7), according to admissibility conditions. Consequently, the substitution of these expressions into Eqs. (5) and (7) implies that $N_1^2 = 0$ and $\boldsymbol{\nabla}\times(\Theta\boldsymbol{n}) = 0$ so that,

$$n_3 N_2^2 - n_2 N_3^2 = 0, \quad n_2^2 + n_3^2 = 1, \tag{11}$$

since the basic absolute vorticity vector $\boldsymbol{W} = (0,0,2\Omega - S)^T$ is time independent and one has $\mathbf{A}\cdot\boldsymbol{W} = \mathbf{0}$. Therefore, the basic buoyancy vector $\Theta\boldsymbol{n}$ must be perpendicular to the streamwise (x_1) direction: A cross-gradient (or radial) density gradient and a vertical one can be present simultaneously. Note that, in the paper by Balbus and Hawley [43], the radial (N_2) and vertical (N_3) frequencies are considered to be independent [see their Eq. (2.10)].

In short, the mean (or base) flow is given by constant shear rate, constant angular velocity, and constant density gradients in vertical and radial directions with the only constraints given by the admissibility conditions; a baroclinic effect is excluded since the total density gradient remains aligned with gravitational acceleration, and no link of Ω to N_i^2, $i = 2,3$ is prescribed.

On the other hand, the induction equation for the mean yields

$$\frac{\partial B_1}{\partial t} = SB_2, \quad \frac{\partial B_2}{\partial t} = 0, \quad \frac{\partial B_3}{\partial t} = 0,$$

so that both the transverse and the axial components of the basic magnetic field are constant, while the streamwise one varies linearly with time,

$$B_1 = B_{10} + B_{20}St, \quad B_2 = B_{20}, \quad B_3 = B_{30}, \tag{12}$$

where the subscript 0 indicates initial value. The Alfvén velocity vector associated with the basic magnetic field $\boldsymbol{B}$ is defined as

$$\boldsymbol{V}_a = \frac{\boldsymbol{B}}{\sqrt{\rho_0\mu_0}}. \tag{13}$$

III. LINEARIZED EQUATIONS FOR THE DISTURBANCES

A. Horizontal and vertical Fourier modes

Single-mode disturbances were called exact solutions by Craik [22], without specifying linearization as an assumption: This is consistent with the fact that a single Fourier mode, even if mean-flow advected, does not interact with itself in the incompressible unbounded case. We prefer to specify linearized here in view of subsequent application to disturbances consisting of a collection of modes, for which nonlinearity is not zero.

The linearized equations for the disturbances $\boldsymbol{u}$ (velocity), $\boldsymbol{b}$ (magnetic field), and θ (buoyancy scalar) for the base flow Eqs. (10)–(12) are easily deduced from Eqs. (3)–(5),

$$\begin{aligned} D_t\boldsymbol{u} &= -\mathbf{A}\cdot\boldsymbol{u} - 2\Omega\boldsymbol{e}_3\times\boldsymbol{u} - \boldsymbol{\nabla}p + \theta\boldsymbol{n} - \boldsymbol{V}_a\times(\boldsymbol{\nabla}\times\boldsymbol{b}),\\ D_t\boldsymbol{b} &= (\boldsymbol{V}\cdot\boldsymbol{\nabla})\boldsymbol{u} + \mathbf{A}\cdot\boldsymbol{b},\\ D_t\theta &= -\left(N_2^2 u_2 + N_3^2 u_3\right), \quad n_3N_2^2 = n_2N_3^2, \end{aligned} \tag{14}$$

with $\boldsymbol{\nabla}\cdot\boldsymbol{u} = 0$ and $\boldsymbol{\nabla}\cdot\boldsymbol{b} = 0$ where $D_t(\cdot) = (\partial_t + Sx_2\partial_{x_1})(\cdot)$. Disturbances are sought in terms of the above-mentioned advected Fourier modes (Refs. [17,22]), also called Kelvin modes or shear waves,

$$\begin{bmatrix} \boldsymbol{u}(\boldsymbol{x},t)\\ p(\boldsymbol{x},t)\\ \frac{1}{\sqrt{\rho_0\mu_0}}\boldsymbol{b}(\boldsymbol{x},t)\\ \theta(\boldsymbol{x},t)\end{bmatrix} = \sum_{\boldsymbol{k}(t)} \begin{bmatrix} \hat{\boldsymbol{u}}(\boldsymbol{k},t)\\ \hat{p}(\boldsymbol{k},t)\\ \hat{\boldsymbol{b}}(\boldsymbol{k},t)\\ \hat{\theta}(\boldsymbol{k},t)\end{bmatrix} \exp[\imath\boldsymbol{k}(t)\cdot\boldsymbol{x}], \tag{15}$$

where the magnetic modes,

$$\hat{\boldsymbol{b}} = \imath\boldsymbol{k}\times\hat{\boldsymbol{a}}$$

have the same dimension as the velocity modes.

The wave vector $\boldsymbol{k}(t)$ satisfies the (eikonal-type) equation: $dk_i/dt = -A_{ji}k_j$ with solution (see Ref. [17]),

$$k_1 = K_1, \quad k_2(t) = K_2 - K_1St, \quad k_3 = K_3, \tag{16}$$

in which capital letters denote initial value $\boldsymbol{K} = \boldsymbol{k}(t=0)$. Using $d\boldsymbol{k}/dt = -\mathbf{A}^T\cdot\boldsymbol{k}$ and $d\boldsymbol{B}/dt = \mathbf{A}\cdot\boldsymbol{B}$, we recover the fact that the Alfvén wave dispersion frequency $\boldsymbol{V}_a\cdot\boldsymbol{k}$ is time independent (see also Ref. [45]) as is the phase of the advected Fourier mode $\boldsymbol{k}\cdot\boldsymbol{x} = \boldsymbol{K}\cdot\boldsymbol{X}$.

The substitution of the solution (15) into (14) leads to a linear seventh-dimensional differential system for $\hat{u}_i, \hat{b}_i$ $(i = 1,2,3)$ and $\hat{\theta}$ (see the Appendix) with the geometrical constraints $\boldsymbol{k}\cdot\hat{\boldsymbol{u}} = 0$ and $\boldsymbol{k}\cdot\hat{\boldsymbol{b}} = 0$ characterizing the fact that both $\boldsymbol{u}$ and $\boldsymbol{b}$ are divergence free. Finally, the spatial Fourier harmonic associated with the linearized part of the potential magnetic induction takes the form

$$\begin{aligned} \hat{\pi}_m &= \imath\,(\boldsymbol{V}_a\cdot\boldsymbol{k})\,\hat{\theta} + N_2^2\hat{b}_2 + N_3^2\hat{b}_3\\ &= \imath(\boldsymbol{V}_a\cdot\boldsymbol{k})\hat{\theta} + \imath N_2^2(k_3\hat{a}_1 - k_1\hat{a}_3) + \imath N_3^2(k_1\hat{a}_2 - k_2\hat{a}_1). \end{aligned} \tag{17}$$

B. Poloidal and toroidal modes

The Craya-Herring frame of reference allows to take the solenoidal property of any vector into account, as a geometric counterpart of the poloidal-toroidal decomposition in physical

space. In addition, effects of shear, rotation, and stratification are more physically reflected in this frame (see Refs. [36,42]). For instance, in the case of stably stratified rotating shearless flow, the use of such a local frame of reference clearly decomposes the velocity-buoyancy field in steady and unsteady motions, the first corresponding to toroidal (without rotation) or quasigeostrophic motion and the second to dispersive inertia-gravity waves (see, e.g., Refs. [42,46]). The local frame is defined by

$$\boldsymbol{e}^{(1)} = \boldsymbol{k}\times\boldsymbol{n}'/\|\boldsymbol{k}\times\boldsymbol{n}'\|, \quad \boldsymbol{e}^{(2)} = \boldsymbol{k}\times\boldsymbol{e}^{(1)}/k, \tag{18}$$

and $\boldsymbol{e}^{(3)} = \boldsymbol{k}/k$, using for $\boldsymbol{n}'$ an arbitrary constant unit vector, specified later, if $\boldsymbol{k}$ is not aligned with $\boldsymbol{n}'$, and it coincides with a fixed frame of reference if not. In this local frame, the coefficients of the velocity $\hat{\boldsymbol{u}}$, the vorticity $\hat{\boldsymbol{\omega}}$, the potential vector $\hat{\boldsymbol{a}}$, and the magnetic field $\hat{\boldsymbol{b}}$ have only two components,

$$\hat{\boldsymbol{u}} = u^{(1)}\boldsymbol{e}^{(1)} + u^{(2)}\boldsymbol{e}^{(2)}, \quad \hat{\boldsymbol{\omega}} = \imath k(u^{(1)}\boldsymbol{e}^{(2)} - u^{(2)}\boldsymbol{e}^{(1)}), \tag{19}$$

$$\hat{\boldsymbol{a}} = a^{(1)}\boldsymbol{e}^{(1)} + a^{(2)}\boldsymbol{e}^{(2)}, \quad \hat{\boldsymbol{b}} = \imath k(a^{(1)}\boldsymbol{e}^{(2)} - u^{(2)}\boldsymbol{e}^{(1)}). \tag{20}$$

For pure shear flow, with no rotation and no stratification, the simplest system of linear equations is found by choosing $\boldsymbol{n}'$ in the cross-gradient direction of the shear or x_2 here. This choice was retained in Ref. [36]. In the present paper, we take $\boldsymbol{n}' = (0,0,1)^T$, which aligns with the rotation axis because it is better adapted to the case of both vertical system vorticity and vertical stratification,

$$\boldsymbol{e}^{(1)} = \left(\frac{k_2}{k_h}, -\frac{k_1}{k_h}, 0\right)^T, \quad \boldsymbol{e}^{(2)} = \left(\frac{k_1k_3}{k_hk}, \frac{k_2k_3}{k_hk}, -\frac{k_h}{k}\right)^T, \tag{21}$$

and hence,

$$\begin{aligned}(u^{(1)},a^{(1)}) &= \frac{k_2}{k_h}(\hat{u}_1,\hat{a}_1) - \frac{k_1}{k_h}(\hat{u}_2,\hat{a}_2),\\ (u^{(2)},a^{(2)}) &= -\frac{k}{k_h}(\hat{u}_3,\hat{a}_3),\end{aligned} \tag{22}$$

where $k_h = \sqrt{k_1^2 + k_2^2}$ is the horizontal wave number. Finally, and for consistency, the definitions,

$$u^{(3)} \equiv ka^{(1)} = -\imath b^{(2)}, \quad u^{(4)} \equiv ka^{(2)} = \imath b^{(1)} \tag{23}$$

are used, and the buoyancy variable $\hat{\theta}$ is scaled to have the same dimension as the velocity modes, or

$$u^{(5)} \equiv -\frac{1}{SR_i}\hat{\theta}, \tag{24}$$

where R_i is the Richardson number defined as (see also Ref. [37]),

$$R_i = \frac{|\nabla\Theta|}{S^2} = \frac{\sqrt{N_2^4 + N_3^4}}{S^2} = \frac{N_2^2}{n_2S^2} = \frac{N_3^2}{n_3S^2}. \tag{25}$$

By setting

$$\eta = \frac{\boldsymbol{V}_a\cdot\boldsymbol{k}}{S} = \left(\frac{\boldsymbol{V}_a\cdot\boldsymbol{k}}{S}\right)_0, \tag{26}$$

i.e., the Alfvén parameter, we obtain the following differential system (see Appendix A):

$$\frac{d\boldsymbol{v}}{d\tau} = \mathbf{C}\cdot\boldsymbol{v}, \tag{27}$$

where

$$\boldsymbol{v} = (u^{(1)},u^{(2)},u^{(3)},u^{(4)},u^{(5)})^T,$$

$$\mathbf{C} = \begin{bmatrix} \frac{k_1k_2}{k_h^2} & -(1+R_\Omega)\frac{k_3}{k} & 0 & \eta & R_i\frac{k_1}{k_h}n_2 \\ \left(R_\Omega + 2\frac{k_1^2}{k_h^2}\right)\frac{k_3}{k} & -\frac{k_1k_2}{k_h^2}\frac{k_3^2}{k^2} & -\eta & 0 & R_i\left(\frac{k_h}{k}n_3 - \frac{k_2k_3}{k_hk}n_2\right) \\ 0 & \eta & \frac{k_1k_2}{k_h^2}\frac{k_3^2}{k^2} & 0 & 0 \\ -\eta & 0 & -\left(1-2\frac{k_1^2}{k_h^2}\right)\frac{k_3}{k} & -\frac{k_1k_2}{k_h^2} & 0 \\ -\frac{k_1}{k_h}n_2 & -\left(\frac{k_h}{k}n_3 - \frac{k_2k_3}{k_hk}n_2\right) & 0 & 0 & 0 \end{bmatrix}. \tag{28}$$

The general solution of the above initial-value problem involves the matrix $\mathbf{g}$, or Green's function such that

$$\boldsymbol{v}(\boldsymbol{k},\tau) = \mathbf{g}(\boldsymbol{k},\tau)\boldsymbol{v}(\boldsymbol{K},0), \tag{29}$$

which is governed by the same equation as $\boldsymbol{v}$, but with universal initial condition $\mathbf{g}(0) = \mathbf{I}_5$. The fact that the trace of the matrix $\mathbf{C}$ is zero implies that the determinant of the matrix $\mathbf{g}$ is unity, $\mathrm{Det}\,\mathbf{g} = 1$, at any time $\tau = St$.

In view of the constant of motion [i.e., Eq. (17)], which can be rewritten as

$$\frac{\imath n_3}{N_3^2}\hat{\pi}_m = \left(\frac{k_h}{k}n_3 - \frac{k_2k_3}{k_hk}n_2\right)u^{(3)} - \frac{k_1}{k_h}n_2u^{(4)} + \eta u^{(5)} = m_0, \tag{30}$$

where

$$m_0 = \left(\frac{K_h}{K}n_3 - \frac{K_2k_3}{K_hK}n_2\right)u_0^{(3)} - \frac{k_1}{K_h}n_2u_0^{(4)} + \eta u_0^{(5)}$$

is a constant, the system (27) reduces to a four-dimensional nonhomogeneous system,

$$\frac{du^{(i)}}{d\tau} = L_{ij}u^{(j)} + h^{(i)} \quad (i,j = 1,2,3,4), \tag{31}$$

where $L_{ij} = C_{ij}$ except

$$\begin{aligned}L_{13} &= C_{13} - \frac{C_{15}}{\eta}\left(\frac{k_h}{k}n_3 - \frac{k_2k_3}{k_hk}n_2\right)\\ &= -\frac{R_i}{\eta}\frac{k_1}{k_h}\left(\frac{k_h}{k}n_3 - \frac{k_2k_3}{k_hk}n_2\right)n_2,\end{aligned}$$

$$L_{14} = C_{14} + \frac{C_{15}}{\eta}\frac{k_1}{k_h}n_2 = \eta - \frac{R_i}{\eta}\frac{k_1^2}{k_h^2}n_2^2,$$
$$L_{23} = C_{23} - \frac{C_{25}}{\eta}\left(\frac{k_h}{k}n_3 - \frac{k_2k_3}{k_hk}n_2\right)$$
$$= -\eta - \frac{R_i}{\eta}\left(\frac{k_h}{k}n_3 - \frac{k_2k_3}{k_hk}n_2\right)^2,$$
$$L_{24} = C_{24} + \frac{C_{25}}{\eta}\frac{k_1}{k_h}n_2 = \frac{R_i}{\eta}\frac{k_1}{k_h}\left(\frac{k_h}{k}n_3 - \frac{k_2k_3}{k_hk}n_2\right)n_2,$$

while

$$h^{(1)} = m_0\frac{R_i}{\eta}\frac{k_1}{k_h}n_2, \quad h^{(2)} = m_0\frac{R_i}{\eta}\left(\frac{k_h}{k}n_3 - \frac{k_2k_3}{k_hk}n_2\right),$$
$$h^{(3)} = h^{(4)} = 0.$$

The nonhomogeneous system satisfied by the linear Green's matrix **g** is reported in Appendix B for the sake of clarity. In the following two sections, we will analyze the system (31) under both axisymmetric and nonaxisymmetric disturbances.

IV. AXISYMMETRIC DISTURBANCES

The limit of $k_1 = 0$ corresponds to the so-called axisymmetric mode. This terminology has no sense from the viewpoint of statistical symmetries preserved by the equations. It originates from the stability analysis of the rotating shear in cylindrical coordinates, for which $k_1 = 0$ corresponds to a zero peripheral wave number. This case yields analytical solutions for disturbances to any plane shear flow, rotating or not, stratified or not, because the wave vector $\boldsymbol{k} = (0, k_2 = K_2, k_3)^T$ is time independent, and hence, matrix **L** is also time independent. In this section, we derive the long-time behavior of the poloidal and toroidal modes that will be used to determine the long-time behavior of energies (kinetic and magnetic) at the $k_1 = 0$ plane (see Sec. VII). Throughout the analytical calculations, we recover and extend some results derived by Balbus and Hawley [43,45] characterizing the MRI and its exponential growth rate.

A. Long-time behavior of the poloidal, toroidal, and potential modes

At $k_1 = 0$, the nonhomogeneous system (27) reduces to

$$\begin{aligned}
&\frac{d}{d\tau}u^{(1)} + [(1+R_\Omega)\sin\alpha]u^{(2)} - \eta u^{(4)} = 0,\\
&\frac{d}{d\tau}u^{(2)} - (R_\Omega\sin\alpha)u^{(1)} + \left(\eta + \frac{R_i}{\eta}\cos^2\gamma\right)u^{(3)}\\
&\quad = \left(\frac{R_i}{\eta}\cos^2\gamma\right)u_0^{(3)} + (R_i\cos\gamma)u_0^{(5)},\\
&\frac{d}{d\tau}u^{(3)} - \eta u^{(2)} = 0,\\
&\frac{d}{d\tau}u^{(4)} + \eta u^{(1)} + \sin\alpha u^{(3)} = 0,
\end{aligned} \tag{32}$$

where

$$\cos\alpha = \frac{k_2}{\sqrt{k_2^2+k_3^2}},$$
$$\cos\gamma = n_3\cos\alpha - n_2\sin\alpha, \tag{33}$$

so that, $\alpha = \gamma$ when there is no horizontal (radial) stratification, i.e., $N_2 = 0$. Obviously, at $k_1 = 0$, there is no effect of the streamwise (azimuthal) component of Alvén vector $\boldsymbol{V}_a$ since the parameter η reduces to

$$\eta = \frac{V_{a2}k_2 + V_{a3}k_3}{S}.$$

An alternative formulation of the nonhomogeneous differential system (33) to a fourth-order ordinary differential equation yields

$$\frac{d^4u^{(2)}}{d\tau^4} + \left(2\eta + \frac{\kappa^2}{S^2}\sin^2\alpha + R_i\cos^2\gamma\right)\frac{d^2u^{(2)}}{d\tau^2}$$
$$+ \eta^2(\eta^2 + R_\Omega\sin^2\alpha + R_i\cos^2\gamma)u^{(2)} = 0,$$

with solution,

$$u^{(2)}(\tau) = \sum_{j=1}^{4}\mathcal{A}_j\exp(\lambda_j\tau), \tag{34}$$

where the coefficient $\mathcal{A}j$ depends on the initial conditions,

$$\begin{aligned}
&\sum_{j=1}^{4}\mathcal{A}_j = u_0^{(2)},\\
&\sum_{j=1}^{4}\mathcal{A}_j\lambda_j^2 = -\left(\eta^2 + \frac{\kappa^2}{S^2}\sin^2\alpha + R_i\cos^2\gamma\right)u_0^{(2)}\\
&\qquad + (\eta R_\Omega\sin\alpha)u_0^{(4)},\\
&\sum_{j=1}^{4}\mathcal{A}_j\lambda_j = (R_\Omega\sin\alpha)u_0^{(1)} - \eta u_0^{(3)} + (R_i\cos\gamma)u_0^{(5)},\\
&\sum_{j=1}^{4}\mathcal{A}_j\lambda_j^3 = -(R_\Omega\sin\alpha)\left(2\eta^2 + \frac{\kappa^2}{S^2}\sin^2\alpha + R_i\cos^2\gamma\right)u_0^{(1)}\\
&\qquad + \eta\left(\eta^2 + R_\Omega^2\sin^2\alpha + R_i\cos^2\gamma\right)u_0^{(3)}\\
&\qquad - (R_i\cos\gamma)\left(\eta^2 + \frac{\kappa^2}{S^2}\sin^2\alpha + R_i\cos^2\gamma\right)u_0^{(5)},
\end{aligned} \tag{35}$$

and

$$(\lambda_{1,2}^2, \lambda_{3,4}^2) = -\frac{1}{2}\left(2\eta^2 + \frac{\kappa^2}{S^2}\sin^2\alpha + R_i\cos^2\gamma\right) \pm \frac{1}{2}\sqrt{\Delta},$$
$$\Delta = \left(R_i\cos^2\gamma + \frac{\kappa^2}{S^2}\sin^2\alpha\right)^2 + 4\eta^2R_\Omega^2\sin^2\alpha \tag{36}$$

are the roots of the algebraic equation,

$$\lambda^4 + \left(2\eta + \frac{\kappa^2}{S^2}\sin^2\alpha + R_i\cos^2\gamma\right)\lambda^2$$
$$+ \eta^2(\eta^2 + R_\Omega\sin^2\alpha + R_i\cos^2\gamma) = 0. \tag{37}$$

The later relation is the same as the dispersion equation (2.19) in Balbus and Hawley [43] but with different notation. The solutions $u^{(1)}$, $u^{(3)}$, and $u^{(4)}$ can be determined by substituting the solution (34) into the system (33), while $u^{(5)}$ can be determined by using the constant of motion (30). For the sake of simplicity, here, we give only the long-time behavior of

these solutions when there is instability (i.e., the MRI, see Balbus and Hawley [43]), i.e., when

$$2\eta^2 + \frac{\kappa^2}{S^2}\sin^2\alpha + R_i\cos^2\gamma \leqslant \sqrt{\Delta},$$

which implies,

$$\eta^2(\eta^2 + R_\Omega\sin^2\alpha + R_i\cos^2\gamma) \leqslant 0. \tag{38}$$

The equality in the above relations characterizes marginal instability (or neutrality). Note that, when the Alfvén parameter vanishes, $\eta = 0$, one recovers the condition for the stratorotational instability (see Salhi *et al.* [37]),

$$\frac{\kappa^2}{S^2}\sin^2\alpha + R_i\cos^2\gamma < 0,$$

which indicates that unmagnetized Keplerian disks [$R_\Omega = -4/3$, $\kappa^2 = \Omega^2 = (4/9)S^2$] or Keplerian disks with a purely azimuthal magnetic field are rather stable under axisymmetric disturbances with or without stratification.

When $(\eta^2 + R_\Omega\sin^2\alpha + R_i\cos^2\gamma) > 0$, one has $\lambda_1 > 0$, $\lambda_2 = -\lambda_1$ and $\lambda_4 = -\lambda_3 = \lambda_3^*$ are pure imaginary,

$$\lambda_1 = \left[-\frac{1}{2}\left(2\eta^2 + \frac{\kappa^2}{S^2}\sin^2\alpha + R_i\cos^2\gamma\right) + \frac{1}{2}\sqrt{\Delta}\right]^{1/2}. \tag{39}$$

In that case, the solution (34) behaves like

$$\begin{aligned}
u^{(2)}(\tau) &= \mathcal{A}_1\exp(\lambda_1\tau), \quad u^{(3)}(\tau) = \frac{\eta}{\lambda_1}u^{(2)}(\tau),\\
u^{(1)}(\tau) &= \frac{\lambda_1^2 + \eta^2 + R_i\cos^2\gamma}{\lambda_1 R_\Omega\sin\alpha}u^{(2)}(\tau),\\
u^{(5)}(\tau) &= \frac{\cos\gamma}{\lambda_1}u^{(2)}(\tau),\\
u^{(4)}(\tau) &= \frac{\lambda_1^2 + \eta^2 + (\kappa^2/S^2)\sin^2\alpha + R_i\cos^2\gamma}{\eta R_\Omega\sin\alpha}u^{(2)}(\tau)
\end{aligned} \tag{40}$$

(i.e., it exhibits an exponential growth) for long times.

B. The MRI growth rate

1. *Purely vertical magnetic field*

We first consider the case with vertical magnetic field ($V_{20} = 0$, $V_{30} \neq 0$) and vertical stratification ($N_2^2 = 0$). For convenience, we introduce the following variables:

$$\sigma = \mathrm{Re}\,\lambda_1, \quad \eta_0 = \frac{V_{30}k_p}{S}, \quad k_\perp^+ = \frac{\sqrt{k_2^2 + k_3^2}}{k_p},$$

where $1/k_p$ is a characteristic vertical length so that the Alfvén parameter η can be rewritten as

$$\eta = \eta_0 k_\perp^+\sin\alpha, \quad \sin\alpha = \frac{k_3}{\sqrt{k_2^2 + k_3^2}}.$$

In that case, the growth rate characterizing the MRI instability, $\sigma = \mathrm{Re}\,\lambda_1 > 0$ takes the form

$$\begin{aligned}
2\sigma^2(\alpha \pm \pi) &= 2\sigma^2(\alpha)\\
&= -\left[2\eta_0^2 k_\perp^{+2}\sin^2\alpha + R_\Omega(1 + R_\Omega)\sin^2\alpha + R_i\cos^2\alpha\right]\\
&\quad + \sqrt{[R_i\cos^2\alpha + R_\Omega(1 + R_\Omega)\sin^2\alpha]^2 + 4\eta_0^2 k_\perp^{+2}R_\Omega^2\sin^4\alpha}.
\end{aligned} \tag{41}$$

Obviously, from the latter relation, one can deduce the angle α at which σ is zero, but it is more simple to deduce this from relation (38) characterizing the condition for the MRI instability. Without stratification, σ vanishes at $\alpha = 0$ and π [i.e., the wave vector aligns with the transverse (radial) direction] provided $k_\perp^+ < -R_\Omega/\eta_0$. In the presence of the vertical stratification, σ takes a zero value at $\alpha = \alpha_1$ or $\alpha = \pi - \alpha_1$ such that

$$\alpha_1 = \arctan\sqrt{\frac{-R_i}{\eta_0^2 k_\perp^{+2} + R_\Omega}}.$$

Consequently, for a finite value of R_i, vertical stratification cannot completely suppress the MRI instability, it restabilizes some modes, i.e., the modes characterized by $0 < \alpha \leqslant \alpha_1$ or $\pi - \alpha_1 \leqslant \alpha < \pi$. On the other hand, the variation in σ with respect to $k_\perp^+$ is extremal, i.e.,

$$\frac{\partial\sigma}{\partial k_\perp^+} = 0 \quad \text{or} \quad \frac{\partial\sigma^2}{\partial k_\perp^+} = 0,$$

at $k_\perp^+ = k_{\perp c}^+$ such that

$$\begin{aligned}
&4\eta_0^2 k_{\perp c}^{+2}\sin^2\alpha\\
&\quad = R_\Omega^2\sin^2\alpha - \frac{[R_i\cos^2\alpha + R_\Omega(1 + R_\Omega)\sin^2\alpha]^2}{R_\Omega^2\sin^2\alpha}.
\end{aligned} \tag{42}$$

The substitution of the above relation into Eq. (42) yields the following expression:

$$\sigma^2(k_{\perp c}^+,\alpha) = \frac{1}{4}\left[1 + \frac{R_i\cos^2\alpha}{R_\Omega\sin^2\alpha}\right]^2\sin^2\alpha \tag{43}$$

(in St units) with $\alpha_1 < \alpha < \pi - \alpha_1$. The maximum value of $\sigma(k_{\perp c}^+,\alpha)$ occurs at $\alpha = \pi/2$, i.e., the Oort A value,

$$\sigma_m = \sigma(k_{\perp c}^+,\alpha_c) = \tfrac{1}{2},$$

(in St units) as in the case without stratification (see, e.g., Ref. [47]). Figure 2 illustrates the variation in σ versus $\cos\alpha$ for the Keplerian disk ($R_\Omega = -4/3$) and $k_\perp^+ = 1$, $k_\perp^+ = 5$, and $k_\perp^+ = k_{\perp c}^+$ [relation (42)]. We indicate that, in several numerical simulations of a Keplerian disk with a purely vertical magnetic field, a characteristic length scale has been taken equal to the most unstable wavelength (see, e.g., Hawley *et al.* [48]),

$$\Lambda_c \equiv \frac{2\pi}{k_{\perp c}^+} = 2\pi\sqrt{\frac{12}{5}}\frac{\eta_0}{k_p} = 2\pi\sqrt{\frac{16}{15}}\frac{V_{30}}{\Omega} = \frac{9.18}{\sqrt{\beta}},$$

so that,

$$\eta_0 = 0.943 k_p\beta^{-1/2}, \tag{44}$$

in which β is a β plasma parameter (i.e., the ratio of the gaz pressure to the magnetic pressure).

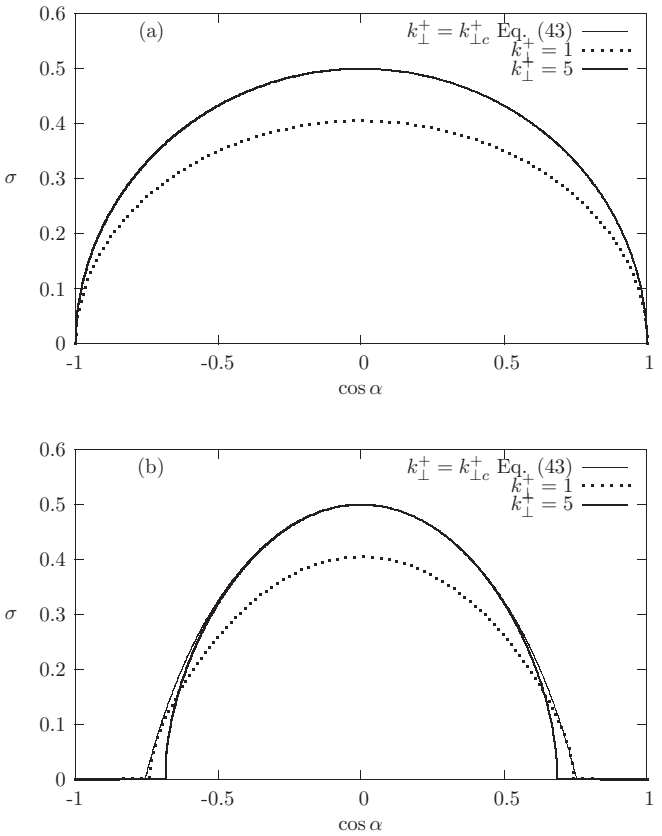

FIG. 2. Variation in the growth rate $\sigma = \mathrm{Re}\,\lambda_1$ (in St units) versus $\cos\alpha$ [Eq. (39)] for a vertically magnetized Keplerian disk under axisymmetric disturbances. (a) Case without stratification $R_i = 0$. (b) Case with vertical stratification $R_i = 1$. The results shown in this figure correspond to $\eta_0 = 4/3$ so that $\beta = 200$ as in the direct numerical simulations by Hawley *et al.* [48]. The domain limited by the $\cos\alpha$ axis and the curve characterizes instability (the MRI instability).

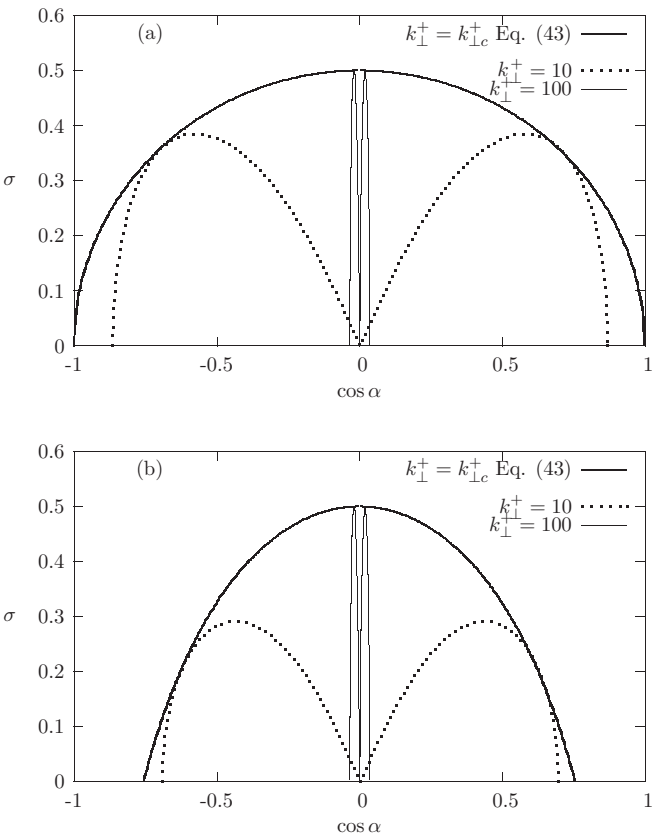

FIG. 3. Variation in the growth rate $\sigma = \mathrm{Re}\,\lambda_1$ (in St units) versus $\cos\alpha$ [Eq. (39)] for a radially magnetized Keplerian disk under axisymmetric disturbances. (a) Case without stratification $R_i = 0$. (b) Case with vertical stratification $R_i = 1$. The results shown in this figure correspond to $\eta_0 = 4/3$ so that $\beta = 200$ as in the direct numerical simulations by Hawley *et al.* [48]. The domain limited by the $\cos\alpha$ axis and the curve characterizes instability (the MRI instability).

2. *Purely radial magnetic field*

In the case with a radial field ($V_{20} \neq 0$, $V_{30} = 0$) and vertical stratification, the condition for instability given by Eq. (38) is rewritten as

$$\left(R_i + \eta_0^2 k_\perp^{+2}\right)\cos^2\alpha + R_\Omega \sin^2\alpha < 0,$$

in which $\eta_0 = V_{20}k_p/S$. Consequently, $\sigma = \mathrm{Re}\,\lambda_1$ takes a zero value for $\alpha = \pi/2$, $0 \leqslant \alpha \leqslant \alpha_2$, or $\pi - \alpha_2 \leqslant \alpha \leqslant \pi$, where

$$\alpha_2 = \arctan\sqrt{-\frac{R_i + \eta_0^2 k_\perp^{+2}}{R_\Omega}}. \tag{45}$$

As illustrated by Fig. 3, the domain of instability is reduced as $k_\perp^+$ increases, and for a given $k_\perp^+$ and R_Ω, vertical stratification restabilizes the modes α such that

$$\arctan\sqrt{-\frac{\eta_0^2 k_\perp^{+2}}{R_\Omega}} < \alpha \leqslant \alpha_2 \quad \text{or}$$

$$\pi - \alpha_2 \leqslant \alpha < \pi - \arctan\sqrt{-\frac{\eta_0^2 k_\perp^{+2}}{R_\Omega}}.$$

The variation in

$$2\sigma^2(\alpha \pm \pi) = 2\sigma^2(\alpha) = -\left[2\eta_0^2 k_\perp^{+2}\cos^2\alpha + R_\Omega(1+R_\Omega)\sin^2\alpha + R_i\cos^2\alpha\right] + \sqrt{\left[R_i\cos^2\alpha + R_\Omega(1+R_\Omega)\sin^2\alpha\right]^2 + 4\eta_0^2 k_\perp^{+2} R_\Omega^2 \cos^2\alpha\,\sin^2\alpha}, \tag{46}$$

with respect to the variable $k_\perp^+$ is extremal at $k_\perp^+ = k_{\perp c}^+$ such that

$$4\eta_0^2 k_{\perp c}^{+2}\cos^2\alpha = -\frac{R_i^2\cos^4\alpha}{R_\Omega^2\sin^2\alpha} - \frac{2R_i(1+R_\Omega)\cos^2\alpha}{R_\Omega} - (1+2R_\Omega)\sin^2\alpha. \tag{47}$$

The substitution of Eq. (47) into Eq. (47) also yields relation (43) with $\alpha_2 < \alpha < \pi/2$ or $\pi/2 < \alpha < \pi - \alpha_2$ since, in this case (i.e., the case with a radial field), the function $\sigma(k_{\perp c}^+,\alpha)$ is not continuous at $\alpha = \pi/2$,

$$\sigma(k_{\perp c}^+,\alpha) \to \tfrac{1}{2} \quad \text{as } \alpha \to (\pi/2)^{\pm}, \quad \sigma(k_{\perp c}^+,\alpha = \pi/2) = 0,$$

as illustrated by Fig. 3 displaying the results for $R_\Omega = -4/3$ (Keplerian disk), $k_\perp^+ = 10$, $k_\perp^+ = 500$, and $k_\perp^+ = k_{\perp c}^+$ [see relation (47)].

3. *Combined effects of vertical and radial magnetic fields*

For combined effects of vertical and radial magnetic fields and combined effects of vertical and radial density gradients, the determination of the α domain in which σ is positive (i.e., indicating a MRI instability), which is characterized by relation (38) or

$$\eta_0^2 k_\perp^{+2} \cos^2(\alpha - \alpha_B) + R_\Omega \sin^2\alpha + R_i \cos^2\gamma < 0 \quad \text{with} \quad \cos(\alpha - \alpha_B) \neq 0,$$

where

$$\eta_0^2 = \frac{k_p}{S}\sqrt{V_{a20}^2 + V_{a30}^2}, \quad \cos\alpha_B = V_{a20}/\sqrt{V_{a20}^2 + V_{a30}^2}$$

requires straightforward calculations. We simply indicate that, at $\alpha = \alpha_B + \pi/2$, σ takes a zero value. In counterpart, it is simpler to determine $\sigma(k_{\perp c}^+,\alpha)$ when there is MRI,

$$\sigma^2(k_{\perp c}^+,\alpha) = \frac{1}{4}\left[1 + \frac{R_i \cos^2\gamma}{R_\Omega \sin^2\alpha}\right]^2 \sin^2\alpha \leqslant \frac{1}{4}, \tag{48}$$

where

$$4\eta_0^2 k_{\perp c}^{+2} \cos^2(\alpha - \alpha_B) = R_\Omega^2 \sin^2\alpha - \frac{[R_i \cos^2\gamma + R_\Omega(1 + R_\Omega)\sin^2\alpha]^2}{R_\Omega^2 \sin^2\alpha}. \tag{49}$$

Accordingly, for magnetized disks under radial stratification (i.e., $N_3 = 0$ so that, $\cos\gamma = \sin\alpha$), the maximal growth rate occurs at $\alpha = \pi/2$ provided $\alpha_B \neq 0$,

$$\sigma_m = \frac{1}{2}\left(1 + \frac{R_i}{R_\Omega}\right) \leqslant \frac{1}{2}. \tag{50}$$

This implies that, for magnetized disks with combined radial and vertical magnetic fields, radial stratification inhibits the MRI instability when $R_i \geqslant -R_\Omega$ so that, $N_2 > \sqrt{3}\Omega$ in the case of a Keplerian disk.

V. NONAXISYMMETRIC DISTURBANCES

The so-called nonaxisymmetric case, or $k_1 \neq 0$, is much more complicated especially if both radial and vertical stratification gradients are simultaneously present ($n_2 \neq 0$ and $n_3 \neq 0$). Therefore, for the sake of brevity and simplicity, we will restrict attention to the case of vertically stratified rotating magnetized sheared flow so that $n_2 = 0$ and $n_3 = 1$. Note that, in previous studies, the stability of the case with nonaxisymmetric disturbances has been investigated numerically (see, e.g., Refs. [45,49,50]). In this section, we use Levinson's theorem to demonstrate that, under nonaxisymmetric disturbances at an infinite vertical wavelength, the solution of the differential system (31) is bounded for sufficiently long times.

When the wave vector is horizontal, i.e.,

$$k_1 = K_1, \quad k_2 = K_2 - k_1\tau, \quad k_3 = 0, \quad k_h = k,$$

there is no effect of rotation (i.e., a 2D limit according to the Taylor-Proudman theorem), and there is no effect of the vertical magnetic field,

$$\eta = \frac{1}{S}(V_{a10}k_1 + V_{a20}K_2) = \frac{V_{a10}k_1 + V_{a20}K_2}{k_p\sqrt{V_{a10}^2 + V_{a20}^2}}\eta_0.$$

In that case, the system (27) reduces to two independent 2D systems,

$$\frac{d}{d\tau}\begin{pmatrix}u^{(1)}\\ u^{(1)}\end{pmatrix} = \underbrace{\begin{bmatrix}\frac{k_1k_2}{k_h^2} & \frac{k_1k_2}{k_h^2}\\ -\eta & -\frac{k_1k_2}{k_h^2}\end{bmatrix}}_{\mathbf{D}}\cdot\begin{pmatrix}u^{(1)}\\ u^{(4)}\end{pmatrix}, \tag{51}$$

$$\frac{d}{d\tau}\begin{pmatrix}u^{(2)}\\ u^{(3)}\end{pmatrix} = \begin{bmatrix}0 & -\left(\eta + \frac{R_i}{\eta}\right)\\ \eta & 0\end{bmatrix}\cdot\begin{pmatrix}u^{(2)}\\ u^{(3)}\end{pmatrix} + \begin{pmatrix}\frac{R_i}{\eta}m_0\\ 0\end{pmatrix}, \tag{52}$$

where

$$m_0 = u_0^{(3)} + \eta u_0^{(5)}.$$

From the latter equation (52), we deduce the following second-order equation,

$$\frac{d^2u^{(2)}}{d\tau^2} + \omega_0^2 u^{(2)} = 0, \quad \omega_0 = \sqrt{\eta^2 + R_i},$$

which indicates stability,

$$\begin{aligned}
u^{(2)}(\tau) &= u_0^{(2)}\cos\omega_0\tau - u_0^{(3)}\frac{\eta}{\omega_0}\sin\omega_0\tau + u_0^{(5)}\frac{R_i}{\omega_0}\sin\omega_0\tau,\\
u^{(3)}(\tau) &= u_0^{(2)}\frac{\eta}{\omega_0}\sin\omega_0\tau + u_0^{(3)}\left(\frac{R_i}{\omega_0^2} + \frac{\eta^2}{\omega_0^2}\cos\omega_0\tau\right)\\
&\quad + u_0^{(5)}\frac{\eta R_i}{\omega_0^2}(1 - \cos\omega_0\tau),\\
u^{(5)}(\tau) &= -u_0^{(2)}\frac{1}{\omega_0}\sin\omega_0\tau + u_0^{(3)}\frac{\eta}{\omega_0^2}(1 - \cos\omega_0\tau)\\
&\quad + u_0^{(5)}\left(\frac{\eta^2}{\omega_0^2} + \frac{R_i}{\omega_0^2}\cos\omega_0\tau\right).
\end{aligned} \tag{53}$$

We conclude that the vertical motion is purely oscillatory with period $2\pi/\sqrt{\eta^2 + R_i}$ (in $\tau = St$ units) since, at $k_3 = 0$, one has

$$\hat{u}_3 = -u^{(2)}, \quad \hat{b}_3 = -b^{(2)} = -\imath k a^{(1)} = -\imath u^{(3)}.$$

The expression of associated vertical kinetic, vertical magnetic, and potential energies will be specified in Sec. VI.

We will now demonstrate by using Levinson's theorem (see Ref. [51], Theorem 1.8.3, p. 35) that the solution of the system (51) is bounded for sufficiently long times.

A. Levinson's theorem

Let the linear differential system,

$$\frac{d\mathbf{\Psi}}{d\tau} = [\mathbf{D_0} + \mathbf{D}_1(\tau) + \mathbf{D}_2(\tau)]\cdot\mathbf{\Psi}, \tag{54}$$

where $\mathbf{D}_0$ is an $n \times n$ constant matrix with n distinct eigenvalues λ_ℓ, $\mathbf{D}_1(x)$ is an $n \times n$ matrix locally absolutely continuous in $[\tau_0, +\infty[$ satisfying

$$\mathbf{D}_1(\tau) \to 0 \quad \text{as } \tau \to \infty, \quad \text{and} \quad \int_{\tau_0}^{\infty} \left|\frac{d\mathbf{D}_1}{d\tau}\right| d\tau < \infty, \tag{55}$$

and $\mathbf{D}_2(\tau)$ an $n \times n$ matrix satisfying

$$\int_{\tau_0}^{\infty} |\mathbf{D}_2(\tau)| d\tau < \infty. \tag{56}$$

Let the eigenvalues $\mu_\ell(\tau)$ of $\mathbf{D}_0 + \mathbf{D}_1(\tau)$ satisfy the dichotomy condition:
For each pair of integers i and j in $[1,n]$ $(i \neq j)$ and for all τ and x such that $\tau_0 \leqslant x \leqslant \tau < \infty$, either
(a)

$$\int_x^{\tau} \mathrm{Re}\{\mu_i(s) - \mu_j(s)\} ds \leqslant q_1,$$

or
(b)

$$\int_x^{\tau} \mathrm{Re}\{\mu_i(s) - \mu_j(s)\} ds \geqslant q_2, \tag{57}$$

where q_1 and q_2 are constants. Then, as $\tau \to \infty$, the differential system (54) has solutions $\mathbf{\Psi}_\ell(\tau)$ $(1 \leqslant \ell \leqslant n)$ with the asymptotic form

$$\mathbf{\Psi}_\ell(\tau) = [\boldsymbol{Y}^{(\ell)} + O(1)] \exp\left[\int_{\tau_0}^{\tau} \mu_\ell(s) ds\right], \tag{58}$$

where $\boldsymbol{Y}^{(\ell)}$ $(1 \leqslant \ell \leqslant n)$ is the eigenvector associated with the eigenvalue λ_ℓ.

B. Application of Levinson's theorem

In view of the above theorem, the matrix $\mathbf{D}$ in system (51) can be decomposed as $\mathbf{D} = \mathbf{D}_0 + \mathbf{D}_1(\tau) + \mathbf{D}_2(\tau)$, where

$$\mathbf{D}_0 = \begin{bmatrix} 0 & \eta \\ -\eta & 0 \end{bmatrix}, \quad \mathbf{D}_1(\tau) = \begin{bmatrix} \frac{k_1 k_2}{k_h^2} & 0 \\ 0 & -\frac{k_1 k_2}{k_h^2} \end{bmatrix}, \tag{59}$$

and $\mathbf{D}_2(\tau) = \mathbf{0}$. The eigenvalues of the constant matrix $\mathbf{D}_0$ are distinct $\lambda_{1,2} = \pm\imath\eta$, and those of the matrix $\mathbf{D}_0 + \mathbf{D}_1(\tau)$ are

$$\mu_{1,2} = \pm\sqrt{\frac{k_1^2 k_2^2}{k_h^4} - \eta^2}. \tag{60}$$

We first show that the dichotomy condition stated in the theorem is satisfied. For $\tau > 1 + |K_2/k_1| = 1 + |\tan\phi|$, the function,

$$\varepsilon(\tau,\phi) = \frac{k_1^2 k_2^2}{k_h^4} = \frac{(\sin\phi - \tau\cos\phi)^2 \cos^2\phi}{[\cos^2\phi + (\sin\phi - \tau\cos\phi)^2]^2},$$

which verifies $\varepsilon(\tau,\phi) = \varepsilon(\tau,\phi \pm \pi)$, decreases approaching zero for long times. Furthermore, one has

$$\max_{\tau\in[0,\infty[} \varepsilon(\tau,\phi) \leqslant \varepsilon\left(1 + \tan\phi,\, 0 \leqslant \phi < \frac{\pi}{2}\right) = \frac{1}{4}.$$

Then, there exists $\tau_0(\eta)$ such that $1 + |\tan\phi| \leqslant \tau_0(\eta) \leqslant \tau < \infty$, for which

$$\varepsilon(\tau,\phi) = \frac{k_1^2 k_2^2}{k_h^4} \leqslant \eta^2, \tag{61}$$

and hence,

$$\mu_{1,2} = \pm\imath\sqrt{\eta^2 - \frac{k_1^2 k_2^2}{k_h^4}}.$$

It follows that $\mathrm{Re}(\mu_1 - \mu_2) = 0$, and then the dichotomy condition stated in the theorem Eq. (57) is satisfied. On the other hand, we show that the condition (55) stated in the theorem is satisfied by the matrix $\mathbf{D}_1(\tau)$. Indeed, one has

$$|(\mathbf{D}_1)_{12}| = |(\mathbf{D}_1)_{21}| = \left|\frac{k_1 k_2}{k_h^2}\right| \to 0,$$

as $\tau \to \infty$ and $|d\mathbf{D}_1/d\tau|$ is impulsively small as $\tau \to \infty$, i.e.,

$$\int_0^{\infty} \left|\frac{d(\mathbf{D}_1)_{12}}{d\tau}\right| d\tau = \int_0^{\infty} \left|\frac{k_1^2}{k_h^2}\left(1 - 2\frac{k_1^2}{k_h^2}\right)\right| d\tau < \infty.$$

Accordingly, we may conclude that, when the wave vector is horizontal (i.e., $k_3 = 0$), there is no sustained growth of fluctuations for sufficiently large times $\tau > \tau_0(\eta)$.

We end this section by briefly considering the case of nonaxisymmetric disturbances with finite vertical wavelength (i.e., $k_3 \neq 0$). We first indicate that the vector $\boldsymbol{h}$ involved in the nonhomogeneous differential system (31) is not impulsively small, i.e., the integral,

$$\int_0^{+\infty} \|\boldsymbol{h}\| d\tau = \left|\frac{m_0 R_i}{\eta}\right| \int_0^{+\infty} \frac{k_h}{k} d\tau$$

does not converge since

$$\int_0^{+\infty} \frac{k_h^2}{k^2} d\tau \leqslant \int_0^{+\infty} \frac{k_h}{k} d\tau,$$

and the integral on the right hand side of the inequality diverges. Therefore, we cannot conclude if the solution of the system (31) is bounded or not even if all the solutions of the homogeneous system are bounded as $\tau \to \infty$ [52]. On the other hand, it is not simpler to see if the five-order matrix $\mathbf{C}$ in the homogeneous system (27) satisfies or not the conditions stated in Levinson's theorem. In counterpart, the Wentzel-Kramers-Brillouin-Jeffreys solution exhibits an oscillatory behavior for sufficiently long times. Indeed, the matrix $\mathbf{L}$ in the nonhomogeneous system (31) can be decomposed into two matrices as $\mathbf{L}_0 + \mathbf{L}_1(\tau)$, where the eigenvalues of the constant matrix $\mathbf{L}_0$ are

$$\lambda_{1,2} = \pm\imath\eta, \quad \lambda_{3,4} = \pm\imath\sqrt{\eta^2 + R_i}, \tag{62}$$

and

$$\lim_{\tau\to\infty} \mathbf{L}_1(\tau) = \mathbf{0}, \quad \lim_{\tau\to\infty} \boldsymbol{h} = \frac{m_0 R_i}{\eta} \boldsymbol{e}_2.$$

As noted by Balbus and Hawley [45], when $\boldsymbol{k}\cdot\boldsymbol{V}/\Omega = \eta S/\Omega$ becomes comparable to the (small) WKB parameter k_1/k_3, the time scale of evolution of the perturbation to evolve is no longer rapid compared with the $\boldsymbol{k}$-changing time scale, WKB methods break down, and numerical integration is required. Further discussions concerning this point will be given in the next section.

Note that the dramatic transient growth can be relevant even when exponential MRI instability occurs as shown by Ref. [53]. The competition between exponentially growing symmetric and transiently growing nonsymmetric perturbations also is important for atmospheric waves. This competition begets a new trend of shear flow dynamics research.

VI. TRANSIENT GROWTH IN THE CASE OF A PURELY AZIMUTHAL MAGNETIC FIELD

Recall that, for axisymmetric disturbances ($k_1 = 0$), there is no effect of an azimuthal magnetic field, while the presence of radial or vertical fields can lead to an MRI instability. The case with a purely azimuthal field has been addressed in several papers to characterize the bypass mechanism for the onset of turbulence in astrophysical disks (see e.g., Ref. [50]). This mechanism could be important since the combination of linearly unstable modes lead to a transient growth, which may become sufficient to trigger nonlinear instabilities (see, e.g., Ref. [50]). In this section, our main purpose is to show that a rapid transient growth (preceding the oscillatory behavior) also can appear for the case of nonaxisymmetric disturbances ($k_1 \neq 0$) with an infinite vertical wavelength (i.e., the $k_3 = 0$ mode that has been addressed in an analytical manner in the previous section) and not only for nonaxisymmetric disturbances with a finite vertical wavelength (i.e., $k_3 \neq 0$ and $k_1 \neq 0$).

A. Spectral density of energy and isotropic initial conditions

To characterize the transient growth, we consider the spectral density of total energy $\mathcal{E}_T$ (kinetic + magnetic + potential), which gives a good estimate of the nonmodal growth of vortex SFHs (see, e.g., Ref. [29]),

$$\mathcal{E}_T = \mathcal{E}_\kappa + \mathcal{E}_m + \mathcal{E}_p, \quad \mathcal{E}_\kappa(t) = \frac{1}{2}(u^{(1)*}u^{(1)} + u^{(2)*}u^{(2)}), \tag{63}$$

$$\mathcal{E}_m(t) = \frac{1}{2}(u^{(3)*}u^{(3)} + u^{(4)*}u^{(4)}), \tag{64}$$

$$\mathcal{E}_p(t) = \frac{R_i}{2}(u^{(5)*}u^{(5)}). \tag{65}$$

Furthermore, by setting $\boldsymbol{v} = (u^{(1)},u^{(2)},u^{(3)},u^{(4)},\sqrt{R_i}u^{(5)})^T$, the spectral density of total energy can be seen as the scalar product,

$$2\mathcal{E}_T(\tau) = \langle \boldsymbol{v}(\tau),\boldsymbol{v}(\tau)\rangle = \langle \mathbf{g}\cdot\boldsymbol{v}(0),\mathbf{g}\cdot\boldsymbol{v}(0)\rangle = \langle \boldsymbol{v}(0),\mathbf{g}^A\mathbf{g}\cdot\boldsymbol{v}(0)\rangle,$$

where $\mathbf{g}^A = \mathbf{g}^{T*}$ is the transconjugate matrix of $\mathbf{g}$. Thus, the spectral density of energy after time τ, relative to the initial energy, is

$$\frac{\mathcal{E}_T(\tau)}{\mathcal{E}_T(0)} = \frac{\langle \boldsymbol{v}(0),\mathbf{g}^A\mathbf{g}\cdot\boldsymbol{v}(0)\rangle}{\langle \boldsymbol{v}(0),\boldsymbol{v}(0)\rangle},$$

and the maximum energy growth $G(\tau)$ obtainable at time τ over all possible initial conditions $\hat{\boldsymbol{v}}(0)$ is (see, e.g., Blackburn *et al.* [54]),

$$G(\tau) = \max_{\boldsymbol{v}(0)} \frac{\langle \boldsymbol{v}(0),\mathbf{g}^A\mathbf{g}\cdot\boldsymbol{v}(0)\rangle}{\langle \boldsymbol{v}(0),\boldsymbol{v}(0)\rangle}.$$

In many studies, the Rayleigh quotient,

$$\mathcal{R}_a = \frac{\langle \boldsymbol{v}(0),\mathbf{g}^A\mathbf{C}\mathbf{g}\cdot\boldsymbol{v}(0)\rangle}{\langle \boldsymbol{v}(0),\mathbf{g}^A\mathbf{g}\cdot\boldsymbol{v}(0)\rangle}$$

is also used to characterize the transient growth (see, e.g., Brandenburg and Dintrans [50]).

In the present paper, we restrict attention to particular initial conditions corresponding to initial isotropic conditions with zero initial magnetic and potential energies and zero initial density and magnetic fluxes,

$$\begin{aligned} u_0^{(1)*}u_0^{(1)} = u_0^{(2)*}u_0^{(2)} = \mathcal{E}_\kappa(0), \quad \mathcal{E}_p(0) = 0, \\ \mathcal{E}_m(0) = 0, \quad \mathrm{Re}\big(u_0^{(i)*}u_0^{(j)}\big) = 0 \quad (i \neq j), \end{aligned} \tag{66}$$

with $(i,j = 1\text{–}5)$. As in several studies (see, e.g., Refs. [48,55]), we use the following Gaussian spectrum:

$$\mathcal{E}_\kappa(0) = \frac{1}{4\pi K^2}\frac{dE_k(0)}{dK} = \frac{C_0}{4\pi k_p^3}\exp\left(-K^2/k_p^2\right), \tag{67}$$

where

$$E_\kappa(0) = \int \mathcal{E}_\kappa(0)d^3\boldsymbol{k} = 4\pi\int_0^\infty K^2\mathcal{E}_\kappa(0)dK$$

is the initial kinetic energy, $C_0 = 4E_\kappa(0)/\sqrt{\pi}$ is a normalization constant, and k_p is the wave number at which the radial spectrum $dE_\kappa(0)/dK$ is maximal. In the present paper, we take $k_p = 20$ in accordance with the direct numerical simulation study of vertically sheared stratified homogeneous turbulence by Holt *et al.* [56].

B. Results and discussion

Due to the initial isotropic conditions [see Eq. (66)], the spectral densities $\mathcal{E}_\kappa(t)$ (kinetic), $\mathcal{E}_m(t)$ (magnetic), and $\mathcal{E}_m(t)$ (potential) can be written as

$$\mathcal{E}_\kappa(t) = \frac{\mathcal{E}_\kappa(0)}{2}\sum_{i=1}^{2}\sum_{j=1}^{2}|g_{ij}|^2, \quad \mathcal{E}_m(t) = \frac{\mathcal{E}_\kappa(0)}{2}\sum_{i=3}^{4}\sum_{j=1}^{2}|g_{ij}|^2,$$

$$\mathcal{E}_p(t) = \frac{R_i\mathcal{E}_\kappa(0)}{2}\sum_{j=1}^{2}|g_{5j}|^2 = \frac{R_i\mathcal{E}_\kappa(0)}{2\eta^2}\frac{k_h^2}{k^2}\sum_{j=1}^{2}|g_{3j}|^2.$$

Recall that the nonhomogeneous differential system for g_{ij} is reported in Appendix B.

From Eq. (54), we deduce that the spectral density of the sum of the poloidal kinetic energy, the poloidal magnetic energy, and the potential energy at $k_3 = 0$ is constant,

$$\mathcal{E}_{pp}(\tau) = \tfrac{1}{2}u^{(2)*}u^{(2)} + \tfrac{1}{2}u^{(3)*}u^{(3)} + \mathcal{E}_p(\tau) = \mathcal{E}_T(0). \tag{68}$$

The spectral density of toroidal kinetic and magnetic energies is computed numerically by integrating (using a fourth-order Runge-Kutta scheme) the 2D system (51). The computation reveals an important transient growth when

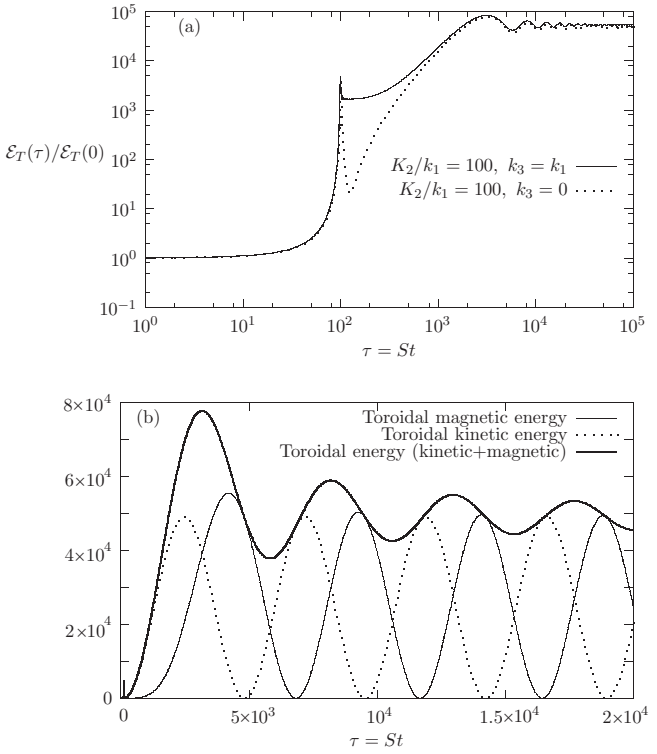

FIG. 4. (a) Time evolution of the spectral density of total energy (kinetic + magnetic + potential) normalized by its initial value in vertically stratified Keplerian disks ($R_\Omega = -4/3$) with a purely azimuthal magnetic field under nonaxisymmetric disturbances for $\eta_0 = V_{a10}k_p/S = 4/3$, $K_h \equiv \sqrt{k_1^2 + K_2^2} = 1$, $k_p = 20$, $K_2/k_1 = 100$, and $R_i = 1$. (b) Time evolution of the spectral density of the toroidal kinetic energy, $u^{(1)*}u^{(1)}/\mathcal{E}_T(0)$ and toroidal magnetic energy $u^{(4)*}u^{(4)}/\mathcal{E}_T(0)$ and their sum $(u^{(1)*}u^{(1)} + u^{(4)*}u^{(4)})/\mathcal{E}_T(0)$ for $k_3 = 0$, $K_h \equiv \sqrt{k_1^2 + K_2^2} = 1$, $\eta_0 = 4/3$, $k_p = 20$, $K_2/k_1 = 100$, and $R_i = 1$.

$K_2/k_1 \gg 1$ as shown by Fig. 4(a) displaying the time development of $\mathcal{E}_T(k_3 = 0)/\mathcal{E}_T(0)$ for $K_2/k_1 = 100$, $\eta_0 = V_{10}k_p/S = 4/3$, $K_h \equiv \sqrt{k_1^2 + K_2^2} = 1$, $k_p = 20$, and $R_i = 1$. Due to the fact that $2\mathcal{E}_{pp}(\tau) = \mathcal{E}_T(0)$ [see Eq. (68)], we conclude that the transient growth of the total energy is due to the toroidal (kinetic and magnetic) energy,

$$2\mathcal{E}_{tt} = u^{(1)*}u^{(1)} + u^{(4)*}u^{(4)}.$$

Furthermore, during the phase $\tau < K_2/k_1$, the ratio $2\mathcal{E}_{tt}(k_3 = 0)/\mathcal{E}_T(0)$ behaves like

$$\frac{K_h^2}{k_h^2} = \frac{1 + (K_2/k_1)^2}{1 + (-\tau + K_2/k_1)^2}, \tag{69}$$

where the above relation characterizes the evolution of the toroidal kinetic energy at $k_3 = 0$ for vertically stratified unmagnetized Keplerian disks (see Salhi *et al.* [37]). This implies that, during the leading phase ($\tau < K_2/k_1$), the toroidal magnetic field is negligible with respect to the toroidal kinetic energy. In counterpart, for $\tau > K_2/k_1$, there is a similar behavior for both $u^{(1)*}u^{(1)}$ and $u^{(4)*}u^{(4)}$ in the sense that they exhibit an oscillatory behavior with high amplitude [see Fig. 4(b)]. This point would definitely be clarified by examining the asymptotic solution (58) given by Levinson's theorem.

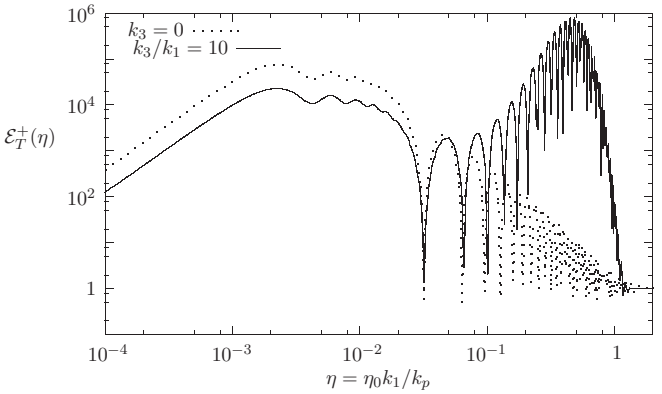

FIG. 5. Variation in the spectral density of total energy (kinetic + magnetic + potential) normalized by its initial value $\mathcal{E}_T^+(\eta) = \mathcal{E}_T^+(\tau = 10^3, \eta)/\mathcal{E}_T(0)$ versus the Alfvén parameter $\eta = \eta_0 k_1/k_p$ for vertically stratified Keplerian disks ($R_\Omega = -4/3$) with a purely azimuthal magnetic field under nonaxisymmetric disturbances for $\eta_0 = V_{a10}k_p/S = 4/3$, $k_p = 20$, $K_2/k_1 = 100$, and $R_i = 1$.

Important results by Chagelishvili *et al.* [57] for the transient dynamics of MHD waves in 2D, incompressible unstratified shear flow, are recovered. For instance, Fig. 3 in Ref. [57] is the same as our Fig. 4(b), with the same $St \sim 100$ threshold value. On the other hand, the initial disturbance, only horizontal and 2D, without magnetic energy, in Ref. [57], is simpler than in our paper. This is illustrated by Fig. 4(b), in which the very long time—long time after the transient growth near $St = 100$—behavior is emphasized. It is shown that the contribution to the total (kinetic + magnetic) energy coming from the toroidal magnetic energy is dominant even if the initial magnetic energy is zero. Of course, the transient growth at $St = 100$, still present, does not appear in Fig. 4(b) because of linear-linear coordinates and very large values of maximum St, $St = 2 \times 10^4$.

For nonaxisymmetric disturbances with finite vertical wavelength ($k_3 \neq 0$), we integrate numerically (using a fourth-order Runge-Kutta scheme) the system (B1) to calculate the spectral density of energies. The present computations show a rapid transient growth for $\mathcal{E}_T(\tau)/\mathcal{E}_T(0)$ [see Fig. 4(a)], in agreement with the previous numerical results [45,50,57]). Although there is a rapid transient growth in the evolution of $\mathcal{E}_T(\tau)/\mathcal{E}_T(0)$ either for $k_3 = 0$ or for $k_3 \neq 0$, the level of energy at large time ($\tau > K_2/k_1$) is not the same as shown by Fig. 5 displaying the variation in $\mathcal{E}_T(\tau)/\mathcal{E}_T(0)$ versus $\eta = \eta_0 k_1/k_p$ for $K_2/k_1 = 100$, $k_3/k_1 = 0, 10$, and $\tau = 1000$. There is more energy at $k_3 = 0$ and low η (or equivalently, at low k_1/k_p since $\eta_0 = 4/3$ is fixed). However, at $\eta \sim 0.5$, the high level of energy cannot occur at $k_3 = 0$.

VII. PREDICTION OF RATIOS OF ENERGIES

Our main purpose in this section is to analyze, by means of the linear theory, the dominant modes of motion by investigating the one-dimensional spectra with respect to the azimuthal and the vertical wave numbers in the case of stratified magnetized Keplerian disks. Although the linear

theory is not able to predict the dynamics of small scales, it remains a useful tool in a qualitative and even in a quantitative manner to characterize the dynamics of large scales (low wave numbers) in which resides a great part of energies due to the interaction between turbulence and the mean-shear flow and/or the body forces. In addition, by considering, as usual in the literature on the subject, the simplest case with a purely vertical magnetic field and with no vertical stratification and gravity, we characterize the long-time behavior of energies at the $k_1 = 0$ plane and attempt to predict the long-time behavior of the ratio of energies.

A. One-dimensional spectra

We consider the spectral density of kinetic energy $\mathcal{E}_\kappa$ and start from the relation,

$$d^3E_\kappa = \mathcal{E}_\kappa d\boldsymbol{k} = \mathcal{E}_\kappa dk_1 dk_2 dk_3, \tag{70}$$

where $E_\kappa = \int \mathcal{E}_\kappa d\boldsymbol{k}$ is the kinetic energy as already indicated. The one-dimensional spectrum of the kinetic energy with respect to the streamwise wave number k_1 is defined as

$$S_\kappa^{(1)}(k_1,t) \equiv \frac{dE_\kappa}{dk_1} = \int\int_{-\infty}^{+\infty} \mathcal{E}_\kappa(\boldsymbol{k},t) dk_2 dk_3 = \int_0^\infty \int_0^{2\pi} \mathcal{E}_\kappa(k_\perp,\alpha,t) k_\perp d\alpha\, dk_\perp, \tag{71}$$

where $(k_\perp,\alpha)$ is a polar coordinates system in the (k_2,k_3) plane,

$$k_2(t) = k_\perp \cos\alpha, \quad k_3 = k_\perp \sin\alpha.$$

The one-dimensional spectrum $S_\kappa^{(3)}(k_3,t)$ with respect to the vertical wave number k_3 can be defined similarly.

Figure 6 shows the one-dimensional spectrum of the magnetic energy $S_m^{(1)}$ for unstratified magnetized Keplerian disks with purely radial, purely azimuthal, or purely vertical magnetic fields at $\tau = 30$ and $\beta = 1600$. As can be expected, the case with the purely vertical field has more energy than the other two cases, and the case with the purely radial field has more energy than the case with the azimuthal field. Recall that, in the latter case, there is stability.

The time development of $S_m^{(1)}(k_1)$ and $S_\kappa^{(1)}(k_1)$ in the case with a purely vertical field indicates that an important contribution to energies comes from the region near the $k_1 = 0$ mode, while the contribution coming from the region near $k_3 = 0$ is not important (see Fig. 7). As indicated previously, at $k_3 = 0$, there is no effect of the Coriolis force and the vertical magnetic field.

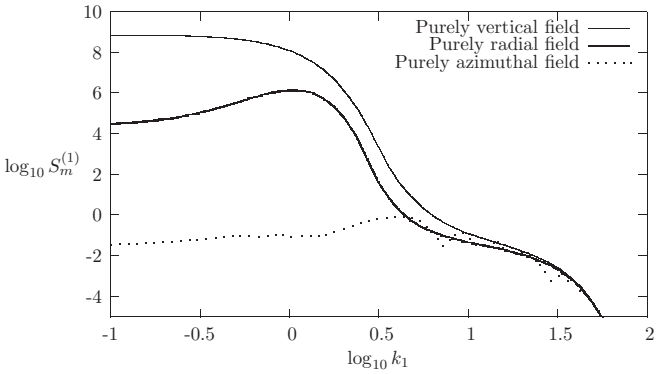

FIG. 6. One-dimensional spectrum $S_m^{(1)}$ in unstratified magnetized Keplerian disks with purely vertical, radial, or azimuthal magnetic fields at $\tau = 30$ and $\beta = 1600$. The initial spectrum used here is described by Eq. (67).

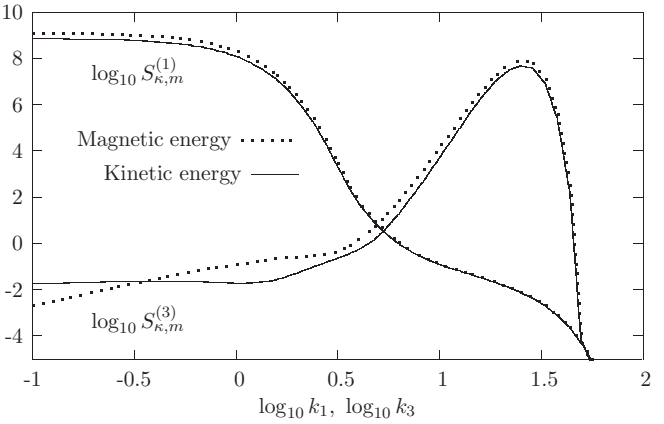

FIG. 7. One-dimensional spectra $S_\kappa^{(1)}$, $S_m^{(1)}$, $S_\kappa^{(3)}$, and $S_m^{(3)}$, in unstratified magnetized Keplerian disks with a purely vertical magnetic field at $\tau = 30$ and $\beta = 1600$. The initial spectrum used here is described by Eq. (67).

Figure 8 shows $S_m^{(1)}(k_1)$ in magnetized stratified Keplerian disks with a purely vertical magnetic field at $\tau = 30$, $R_i = 1$, and $\beta = 1600$. The results characterizing the case without stratification also are reported for comparison. As can be expected, stratification reduces the energy especially at the intermediate wave numbers. This can be explained by the fact that the vertical stratification restabilizes some modes but does not affect the most unstable mode that corresponds to the vertical wave vector (see Sec. IV B).

B. Two-dimensional energy components in the streamwise direction

Because the region near $k_1 = 0$ has an important contribution to energy, in the presence of a vertical magnetic field, it seems interesting to analyze the behavior of the following

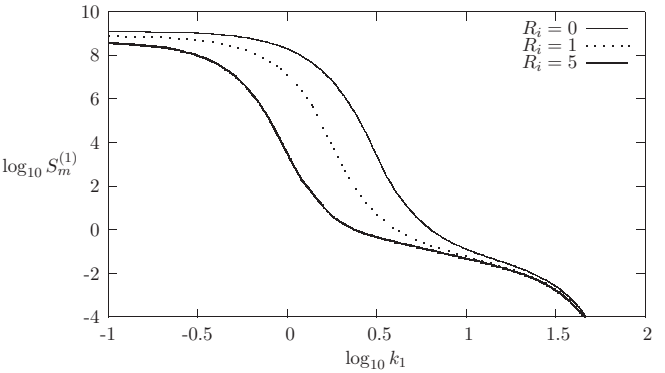

FIG. 8. Effects of vertical stratification on the one-dimensional spectrum $S_m^{(1)}$ for magnetized Keplerian disks with a purely vertical magnetic field at $\tau = 30$. The initial spectrum used here is described by Eq. (67).

limit:

$$E_k L^{(1)} = \pi \lim_{k_1 \to 0} S_k^{(1)}(k_1,t), \tag{72}$$

which represents the product of the kinetic energy E_κ by the associated integral length scale in the streamwise direction $L^{(1)}$ also called the 2D energy components (see, e.g., Refs. [15,36]).

We consider, for the sake of clarity and as performed in most of the literature on the subject, the simplest case of an unstratified magnetized Keplerian disk with a purely vertical magnetic field. From the solution (40), giving the long-time behavior of the poloidal, toroidal, and buoyancy modes at $k_1 = 0$, we deduce the long-time behavior of the spectral density of the kinetic energy $\mathcal{E}_k^{(1)}$ and the magnetic energy $\mathcal{E}_m^{(1)}$,

$$\mathcal{E}_k^{(1)}(k_\perp^+,\alpha) = \mathcal{A}_1^2\left[1 + \frac{\left(\sigma_0^2 + \eta_0^2 k_\perp^{+2}\right)^2}{\sigma_0^2 R_\Omega^2}\right]\exp(2\sigma_0\tau\ \sin\alpha),$$

$$\mathcal{E}_m^{(1)}(k_\perp^+,\alpha) = \mathcal{A}_1^2\left\{\frac{\eta_0^2 k_\perp^{+2}}{\sigma_0^2} + \frac{\left[\sigma_0^2 + \eta_0^2 k_\perp^{+2} + R_\Omega\left(R_\Omega+1\right)\right]^2}{\eta_0^2 k_\perp^{+2} R_\Omega^2}\right\} \times \exp(2\sigma_0\tau\ \sin\alpha), \tag{73}$$

where

$$\sigma_0^2 = \frac{\lambda_1^2}{\sin^2\alpha} = -\frac{1}{2}\left[\eta_0^2 k_\perp^{+2} + R_\Omega(R_\Omega+1)\right] + \frac{1}{2}\sqrt{\Delta},$$

and

$$\mathcal{A}_1^2 = \frac{1}{16\sigma_0^2\Delta}\left\{\sigma_0^2[R_\Omega(R_\Omega+1) - \sqrt{\Delta}]^2 + R_\Omega^2\left[2\eta_0^2 k_\perp^{+2} + R_\Omega(R_\Omega+1) - \sqrt{\Delta}\right]^2\right\}\mathcal{E}_\kappa(0),$$

$$\Delta = R_\Omega^2(R_\Omega+1)^2 + 4\eta_0^2 k_\perp^{+2} R_\Omega^2.$$

Accordingly, the long-time behavior of the streamwise 2D kinetic energy takes the form

$$E_\kappa L^{(1)} = 2\pi\int_0^\infty\int_0^\pi \mathcal{E}_\kappa^{(1)} k_\perp d\alpha\, dk_\perp \to 2\pi\int_0^{k_{\perp\ell}}\int_0^\pi \mathcal{E}_\kappa^{(1)}(\tau) k_\perp d\alpha\, dk_\perp,$$

where $k_{\perp\ell}$ denotes the particular value of $k_\perp$ at which the MRI instability vanishes [i.e., $\sigma_0(k_{\perp\ell}) = 0$, see Eq. (38)],

$$k_{\perp\ell} = k_p k_{\perp\ell}^+ = \frac{\sqrt{-R_\Omega}}{\eta_0} k_p.$$

The integration with respect to the angular variable is performed analytically,

$$E_\kappa L^{(1)} \sim \int_0^{k_{\perp\ell}} \mathcal{A}_1^2\left[1 + \frac{\left(\sigma_0^2 + \eta_0^2 k_\perp^{+2}\right)^2}{\sigma_0^2 R_\Omega^2}\right] \times [\mathbf{I}_0(2\sigma_0\tau) + \mathbf{L}_0(2\sigma_0\tau)]\mathcal{E}_\kappa^{(1)}(0) k_\perp dk_\perp \to \int_0^{k_{\perp\ell}} \mathcal{A}_1^2\left[1 + \frac{\left(\sigma_0^2 + \eta_0^2 k_\perp^{+2}\right)^2}{\sigma_0^2 R_\Omega^2}\right] \times \frac{\exp(2\sigma_0\tau)}{\sqrt{\sigma_0\tau}}\mathcal{E}_\kappa^{(1)}(0) k_\perp dk_\perp, \tag{74}$$

whereas, the integration over the modulus $k_\perp$ is performed numerically. Here, $\mathbf{I}_n\,(2\sigma t)$ is the Bessel function, and $\mathbf{L}_n\,(2\sigma t)$ is the modified Struve function (see, e.g., Refs. [58,59]), and $\mathcal{E}_\kappa^{(1)}(0)$ represents the initial spectrum at $k_1 = 0$. Similar expressions can be obtained for the 2D Reynolds stresses, the 2D Maxwell stresses, and the 2D magnetic fluxes. For instance, we report here only the expression of the 2D magnetic energy $E_m L_m^{(1)}$, the 2D Reynolds shear stress $E_{\kappa 12} L_{\kappa 12}^{(1)}$, and the 2D Maxwell stress $E_{m12} L_{m12}^{(1)}$,

$$\begin{aligned} E_m L_m^{(1)} &\sim \int_0^{k_{\perp\ell}} \mathcal{A}_1^2\left\{\frac{\eta_0^2 k_\perp^{+2}}{\sigma_0^2} + \frac{\left[\sigma_0^2 + \eta_0^2 k_\perp^{+2} + R_\Omega(R_\Omega+1)\right]^2}{\eta_0^2 k_\perp^{+2} R_\Omega^2}\right\}\frac{\exp(2\sigma_0\tau)}{\sqrt{\sigma_0\tau}}\mathcal{E}_\kappa^{(1)}(0) k_\perp dk_\perp, \\ E_{\kappa 12} L_{\kappa 12}^{(1)} &\sim -\int_0^{k_{\perp\ell}} \mathcal{A}_1^2 \frac{\left(\sigma_0^2 + \eta_0^2 k_\perp^{+2}\right)}{2R_\Omega\sigma_0}\frac{\exp(2\sigma_0\tau)}{\sqrt{\sigma_0\tau}}\mathcal{E}_\kappa^{(1)}(0) k_\perp dk_\perp, \\ E_{m12} L_{m12}^{(1)} &\sim \int_0^{k_{\perp\ell}} \mathcal{A}_1^2 \frac{\left[\sigma_0^2 + \eta_0^2 k_\perp^{+2} + R_\Omega(R_\Omega+1)\right]}{2R_\Omega\sigma_0}\frac{\exp(2\sigma_0\tau)}{\sqrt{\sigma_0\tau}}\mathcal{E}_\kappa^{(1)}(0) k_\perp dk_\perp. \end{aligned} \tag{75}$$

The above integrals are computed numerically for $\beta(=$ 50–1600) as in the numerical paper by Hawley *et al.* [48]. The numerical results reveal that the ratio,

$$R_{m\kappa}^{(1)} = \frac{E_m L_m^{(1)}}{E_\kappa L_\kappa^{(1)}}$$

reaches an equilibrium value $R_{m\kappa}^{(1)} = 1.667$, which is insensitive to parameter β. Such an equilibrium value is smaller than in the simulations with a uniform vertical field reported in Hawley *et al.* [53]. In fact, from their Table 2, giving the results obtained for $\beta = 400$, we deduce the value $R_{m\kappa} = E_m/E_\kappa = 2.267$. Also, the present simple model underestimates the ratio of the Maxwell stress to the Reynolds stress since it yields the equilibrium value,

$$R_{12m\kappa}^{(1)} = \frac{E_{m12} L_{m12}^{(1)}}{E_{\kappa 12} L_{\kappa 12}^{(1)}} = 1.667,$$

while the simulations by Hawley *et al.* [53] yield $R_{12m\kappa} = E_{m12}/E_{\kappa 12} = 5.37$, and in the recent simulations with high resolution by Bodo *et al.* [6], it is about 5. In the latter numerical paper, the following correlations:

$$\tan\psi = -\frac{E_{m12}}{E_{m22}}, \quad R_{12mm} = \frac{E_{m12}^2}{E_{m11}E_{m22}}$$

are about 1.2 and 0.5, respectively (see the third panels in their Fig. 3), whereas, in the simulations by Hawley *et al.* [53], $\tan\psi = 0.799$ and $R_{12mm} = 0.4864$ (deduced from their Table 2). As for the present simple model, it yields

$$\tan\psi^{(1)} = -\frac{E^{(1)}_{m12}}{E^{(1)}_{m22}} = 1, \quad R^{(1)}_{12mm} = \frac{\left(E^{(1)}_{m12}\right)^2}{E^{(1)}_{m11}E^{(1)}_{m22}} = 1.$$

It should be noted that, in the simulations by Hawley *et al.* [48] for the case with zero net vertical field [$\boldsymbol{B} = B_3(x_2)\boldsymbol{e}_3$, $B_3 \sim \sin x_2$], it is found that R_{mk} varies between 1.4 and 2.2, and $R_{12m\kappa}$ varies between 1.4 and 2.2.

To end this section, we indicate that the equilibrium value for ratios of energies is insensitive to viscosity, at least, when the magnetic Prandtl number is unity. In fact, in that case, we multiply the expression of the spectral density of energies for an inviscid and nondiffusive fluid by the factor $[\exp(-2\nu k_\perp^2/S)]$, where ν is the kinematic viscosity.

VIII. CONCLUDING REMARKS

In this paper, we have recovered and have extended previously known results concerning the behavior of a fluid submitted to simultaneous conditions of rotation, shear, stratification, and magnetic field under the Boussinesq approximation for an inviscid and nondiffusive fluid.

Because of the presence of the Lorentz force as a magnetic feedback in the momentum equation, the use of Ertel's theorem for the absolute potential vorticity no longer works. In counterpart, the potential magnetic induction (i.e., the scalar product of the magnetic vector by the density gradient) constitutes a Lagrangian invariant for an inviscid and nondiffusive fluid.

Because the base flow must satisfy the admissibility conditions, only radial and/or vertical density gradients can be taken into account: The admissibility conditions exclude the presence of a streamwise (or azimuthal) component of the density gradient. In addition, the radial and vertical stratification intensities N_2^2 and N_3^2 are not independent since the buoyancy vector field $\Theta\boldsymbol{n} = (N_2^2 x_2 + N_3^2 x_3)\boldsymbol{n}$ is irrotational, yielding $n_2 N_3^2 = n_3 N_2^2$.

We have used the spectral linear theory in terms of Fourier (or Kelvin) time-advected modes to describe the fluid evolution within the shearing box model. This model also is very popular in astrophysics as a useful tool to study accretion disks. In a local frame attached to the wave vector, the linear differential system reduces to a fifth-dimensional one for the toroidal ($u^{(1)}$,$u^{(3)}$), poloidal ($u^{(2)}$,$u^{(4)}$), and potential $u^{(5)}$ modes, or equivalently, for the fifth-rank Green matrix $\mathbf{g}$ introduced for universal initial conditions. The use of the constant of motion [relation (17)], which is a consequence of the fact that the magnetic potential is a Lagrangian invariant for an inviscid and nondiffusive fluid, permits reducing the linear system to a fourth-dimensional nonhomogeneous differential system for the toroidal and poloidal modes.

We have performed a stability analysis for both infinite wavelength ($k_1 = 0$ or axisymmetric disturbances) and finite streamwise wavelength ($k_1 \neq 0$ or nonaxisymmetric disturbances).

In the former case (i.e., $k_1 = 0$), previous results concerning the MRI instability are recovered and are extended considering the combined effects of radial and vertical magnetic fields and combined radial and vertical density gradients. The dependence of the MRI growth rate on the rotation and Richardson numbers for any orientation and any modulus of the wave vector in the $k_1 = 0$ plane has been derived [see Eq. (48)]. Vertical stratification restabilizes some modes, but it does not inhibit the MRI instability, and its maximal growth rate is not modified by stratification, $\sigma_m = 1/2$ (in St units), i.e., the Oort A value (Balbus and Hawley [45]). In counterpart, radial stratification can suppress the MRI instability (see the end of Sec. IV B). We also have derived the long-time behavior of the toroidal, poloidal, and potential modes when there is an MRI instability [see Eq. (40)]. The analytical expression has been used to investigate the spectral density of energy at $k_1 = 0$, as well as the streamwise 2D energy components since the SLT approach can be used to predict statistics (see below). By taking the effect of rigid boundary conditions in the radial direction into account and considering vertical stratification and purely vertical magnetic field, we have derived a dispersion relation [see Eq. (C4)] in Appendix C similar to the one derived in the unbounded case Eq. (37), but in which the radial wave number takes discrete values.

As mentioned in most of the literature on the subject, for nonaxisymmetric solutions, a purely analytic treatment of the shearing sheet model is generally difficult since the solutions exhibit a complicated temporal behavior. The application of Levinson's theorem in the case of an infinite vertical wavelength ($k_3 = 0$) corroborates this, especially the analysis related to the dichotomy conditions stated in the theorem. Although this analysis is restricted to the $k_3 = 0$ mode, a closer examination of the solution (58) given by the theorem provides additional theoretical insight, especially in the case with a purely azimuthal magnetic field. In fact, under axisymmetric disturbances ($k_1 = 0$), there is no effect of the azimuthal magnetic field, and the solution of system (33) is purely oscillatory and cannot lead to a transient growth in the case of Keplerian disks (see Salhi *et al.* [37]). In counterpart, at $k_3 = 0$, the spectral density of energy exhibits a rapid transient growth provided $K_2/k_1 \gg 1$ as shown in Sec. VI and summarized here. For initial isotropic conditions, the time evolution of the spectral density of total energy (kinetic + magnetic + potential) is considered. At $k_3 = 0$, the vertical motion is purely oscillatory, and the vertical (kinetic + magnetic) energy plus the potential energy does not evolve with time and remains equal to its initial value. The horizontal motion can induce a rapid transient growth, provided $K_2/k_1 \gg 1$ (see Figs. 4 and 5). This rapid growth is due to the aperiodic velocity vortex mode that behaves like K_h/k_h. After the leading phase ($\tau > K_2/k_1 \gg 1$), the horizontal magnetic energy and the horizontal kinetic energy exhibit a similar (oscillatory) behavior yielding a high level of total energy [see Fig. 4(b)]. The bypass mechanism for the onset of turbulence in the case with a purely azimuthal field would be characterized even better by analyzing the wave-vortex coupling as performed in previous papers for stratified unmagnetized Keplerian disks (see Refs. [29,37]).

The contribution to energies coming from the modes $k_1 = 0$ and $k_3 = 0$ is addressed by computing one-dimensional spectra for an initial Gaussian dense spectrum. For a magnetized Keplerian disk with a purely vertical field, it is found that an important contribution to magnetic and kinetic energies comes from the region near $k_1 = 0$, while the contribution coming from the region near $k_3 = 0$ is not dominant (see Fig. 7). Accordingly, the streamwise 2D energy, or equivalently, the limit at $k_1 = 0$ of the streamwise one-dimensional spectra of energies, is then computed. In these computations, the spectral density of energy is obtained analytically as well as the integration with respect to the α angle (i.e., the angle between the radial direction and the wave vector in the $k_1 = 0$ plane), whereas, the integration over the modulus $k_\perp$ is performed numerically. It is found that the ratios of energies, such as the ratio of magnetic to kinetic energies reach an equilibrium value that is insensitive to the β parameter and the viscosity. The comparison of the ratios of these 2D quantities with their three-dimensional counterparts yielded by previous direct numerical simulations shows a quantitative agreement.

APPENDIX A: DERIVATION OF THE DIFFERENTIAL SYSTEM IN A LOCAL FRAME

The first equation in Eq. (15) can be rewritten as

$$\dot{\hat{\boldsymbol{u}}} = -\mathbf{A}\cdot\hat{\boldsymbol{u}} - 2\Omega\boldsymbol{e}_3 \times \hat{\boldsymbol{u}} - \imath\hat{p}\boldsymbol{k} + \hat{\theta}\boldsymbol{n} - k^2\boldsymbol{V}_a \times \hat{\boldsymbol{a}},$$

or equivalently,

$$\begin{aligned}\dot{u}^{(\alpha)}\boldsymbol{e}^{(\alpha)} = {} & -u^{(\alpha)}\dot{\boldsymbol{e}}^{(\alpha)} - u^{(\alpha)}\mathbf{A}\cdot\boldsymbol{e}^{(\alpha)} - 2\Omega u^{(\alpha)}(\boldsymbol{n}' \times \boldsymbol{e}^{(\alpha)}) \\ & - \imath k\hat{p}\boldsymbol{e}^{(3)} + \hat{\theta}\boldsymbol{n} - k^2 a^{(\alpha)}\boldsymbol{V}_a \times \boldsymbol{e}^{(\alpha)}\end{aligned}$$

since $\hat{\boldsymbol{b}} = \imath\boldsymbol{k} \times \hat{\boldsymbol{a}}$ and $\hat{\boldsymbol{u}} = u^{(\alpha)}\boldsymbol{e}^{(\alpha)}$ and $\hat{\boldsymbol{a}} = a^{(\alpha)}\boldsymbol{e}^{(\alpha)}$ ($\alpha = 1,2$). Recall that $\mathbf{n} = (0,n_2,n_3)^T$, $\mathbf{n}' = (0,0,1)^T$, and $A_{ij} = S\delta_{i1}\delta_{j1}$. Due to the fact that $(\boldsymbol{e}^{(1)},\boldsymbol{e}^{(2)},\boldsymbol{e}^{(3)})$ is an orthonormal base [see Eq. (18)], the product by $\boldsymbol{e}^{(\beta)}$ ($\beta = 1,2$) of the two sides of the above equation yields

$$\dot{u}^{(\beta)} = m_{\beta\alpha}u^{(\alpha)} + (\boldsymbol{n}\cdot\boldsymbol{e}^{(\beta)})\hat{\theta} - k^2 a^{(\alpha)}\boldsymbol{V}_a\cdot[\boldsymbol{e}^{(\alpha)} \times \boldsymbol{e}^{(\beta)}], \quad \text{(A1)}$$

where

$$m_{\beta\alpha} = -\left[e_i^{(\beta)}\dot{e}_i^{(\alpha)} + e_i^{(\beta)}A_{ij}e_j^{(\alpha)} + 2\Omega(\boldsymbol{n}' \times \boldsymbol{e}^{(\alpha)})_i e_i^{(\beta)}\right].$$

Thus,

$$-e_i^{(\beta)}A_{ij}e_j^{(\alpha)} = S\begin{bmatrix} \frac{k_1k_2}{k_h^2} & -\frac{k_2^2}{k_h^2}\frac{k_3}{k} \\ \frac{k_1^2}{k_h^2}\frac{k_3}{k} & -\frac{k_1k_2}{k_h^2}\frac{k_3^2}{k^2}\end{bmatrix}, \quad \text{(A2)}$$

$$-2\Omega(\boldsymbol{n} \times \boldsymbol{e}^{(\alpha)})_i e_i^{(\beta)} = 2\Omega\begin{bmatrix} 0 & \frac{k_3}{k} \\ -\frac{k_3}{k} & 0\end{bmatrix}, \quad \text{(A3)}$$

and

$$-e_i^{(1)}\dot{e}_i^{(2)} = S\begin{bmatrix} 0 & -\frac{k_1^2}{k_h^2}\frac{k_3}{k} \\ \frac{k_1^2}{k_h^2}\frac{k_3}{k} & 0\end{bmatrix}. \quad \text{(A4)}$$

Accordingly, the matrix $\mathbf{m}$ takes the form

$$\begin{aligned} m_{\beta\alpha} &= S\begin{bmatrix} \frac{k_1k_2}{k_h^2} & -(1+R_\Omega)\frac{k_3}{k} \\ \left(R_\Omega + 2\frac{k_1^2}{k_h^2}\right)\frac{k_3}{k} & -\frac{k_1k_2}{k_h^2}\frac{k_3^2}{k^2}\end{bmatrix}, \\ -k^2 a^{(\alpha)}\boldsymbol{V}_a\cdot[\boldsymbol{e}^{(\alpha)} \times \boldsymbol{e}^{(\beta)}] &= S\eta(-u^{(3)}\delta_{1\beta} + u^{(4)}\delta_{2\beta}),\end{aligned} \quad \text{(A5)}$$

and

$$(\boldsymbol{n}\cdot\boldsymbol{e}^{(\beta)})\hat{\theta} = SR_i\left[n_2\frac{k_1}{k_h}\delta_{1\beta} + \left(n_3\frac{k_h}{k} - n_2\frac{k_2k_3}{k_hk}\right)\delta_{2\beta}\right]u^{(5)},$$

where $\eta = \boldsymbol{V}_a\cdot\boldsymbol{k}/S$, In a similar manner, we transform the second and third equations in Eq. (15).

APPENDIX B: NONHOMOGENEOUS DIFFERENTIAL SYSTEM FOR THE GREEN MATRIX

The nonhomogeneous differential system for the matrix $\mathbf{g}$ such that $\hat{\boldsymbol{u}}(t) = \mathbf{g}\cdot\hat{\boldsymbol{u}}(0)$, is deduced from the nonhomogeneous system (31),

$$\frac{dg_{ij}}{d\tau} = L_{im}g_{mj} + Q_{ij}, \quad (i,m = 1\text{–}4) \quad (j = 1,2,\ldots,5), \quad \text{(B1)}$$

where $Q_{ij} = 0$ except

$$\begin{aligned} Q_{13} &= \frac{C_{15}}{\eta}\left(\frac{K_h}{K}n_3 - \frac{K_2k_3}{K_hK}n_2\right) \\ &= \frac{R_i}{\eta}\frac{k_1}{k_h}\left(\frac{K_h}{K}n_3 - \frac{K_2k_3}{K_hK}n_2\right)n_2, \\ Q_{14} &= -\frac{C_{15}}{\eta}\frac{k_1}{k_h}n_2 = \frac{R_i}{\eta}\frac{k_1^2}{k_hK_h}n_2^2, \\ Q_{15} &= \frac{C_{15}}{\eta} = R_i\frac{k_1}{k_h}n_2, \\ Q_{23} &= \frac{C_{25}}{\eta}\left(\frac{K_h}{K}n_3 - \frac{K_2k_3}{K_hK}n_2\right) \\ &= \frac{R_i}{\eta}\left(\frac{k_h}{k}n_3 - \frac{k_2k_3}{k_hk}n_2\right)\left(\frac{K_h}{K}n_3 - \frac{K_2k_3}{K_hK}n_2\right), \\ Q_{24} &= -\frac{C_{25}}{\eta}\frac{k_1}{K_h}n_2 = -\frac{R_i}{\eta}\frac{k_1}{K_h}\left(\frac{k_h}{k}n_3 - \frac{k_2k_3}{k_hk}n_2\right)n_2, \\ Q_{25} &= \frac{C_{25}}{\eta} = R_i\left(\frac{k_h}{k}n_3 - \frac{k_2k_3}{k_hk}n_2\right).\end{aligned}$$

The component g_{5j} ($j = 1,2,\ldots,5$) is obtained from Eq. (30),

$$\begin{aligned} g_{5j} = {} & \delta_{5j} - \frac{1}{\eta}\left(\frac{k_h}{k}n_3 - \frac{k_2k_3}{k_hk}n_2\right)g_{3j} + \frac{1}{\eta}\frac{k_1}{k_h}n_2g_{4j} \\ & + \frac{1}{\eta}\left(\frac{K_h}{K}n_3 - \frac{K_2k_3}{K_hK}n_2\right)\delta_{3j} - \frac{1}{\eta}\frac{k_1}{K_h}n_2\delta_{4j}. \end{aligned} \quad \text{(B2)}$$

APPENDIX C: EFFECTS OF RIGID BOUNDARY CONDITIONS ON THE MRI

We now analyze the effect of rigid boundary conditions on the MRI considering the case where the fluid is contained between vertical planes at $x_2 = 0$ and $x_2 = L$ and remains unbounded with respect to the streamwise and vertical directions. Physically, such a geometrical configuration would rather be supported by a Taylor-Couette flow with an axial magnetic field such that ($r \ll R_1 \ll L$, i.e., long concentric cylinders with small radii and very short distances between the two cylinders). For the sake of simplicity, we consider the case with a vertical stratification and a purely vertical magnetic field. In that case, the linearized equations for the disturbances take the form

$$
\begin{aligned}
&D_t u_1 = -(S-2\Omega)u_2 - \partial_{x_1} p + \frac{V_{az}}{\sqrt{\rho_0\mu_0}}(\partial_{x_3} b_1 - \partial_{x_1} b_3),\\
&D_t u_2 = -2\Omega u_1 - \partial_{x_2} p + \frac{V_{az}}{\sqrt{\rho_0\mu_0}}(\partial_{x_3} b_2 - \partial_{x_2} b_3),\\
&D_t u_3 = -\partial_{x_3} p + \theta, \quad D_t b_1 = S b_2 + \sqrt{\rho_0\mu_0} V_{az}\partial_{x_3} u_1, \quad \text{(C1)}\\
&D_t b_2 = \sqrt{\rho_0\mu_0} V_{az}\partial_{x_3} u_2, \quad D_t b_3 = \sqrt{\rho_0\mu_0} V_{az}\partial_{x_3} u_3,\\
&\partial_{x_i} u_i = 0, \quad \partial_{x_i} b_i = 0, \quad D_t \pi_m = 0,
\end{aligned}
$$

in which $\pi_m = [N_v^2 b_3 + \sqrt{\rho_0\mu_0}\partial_{x_3}\theta]$ is the linearized part of the magnetic potential and $D_t(\cdot) = \partial_t(\cdot) + S x_2 \partial_{x_1}(\cdot)$. In accordance with previous classical hydrodynamic stability analyses (see, e.g., Drazin and Reid [60]), we will use the following dimensionless variables $x = x_1/(LS/2\Omega)$, $y = x_2/L$, $z = x_3/(LS/2\Omega)$, $t' = 2\Omega t$, $u = u_1/(2\Omega L)$, $v = u_2/(LS)$, $w = u_3/(2\Omega L)$, $p' = p/(2\Omega S L^2)$, and $\theta' = \theta/(4\Omega^2 L)$,

$$
b_1' = \frac{b_1}{2\Omega L\sqrt{\rho_0\mu_0}}, \quad b_2' = \frac{b_2}{LS\sqrt{\rho_0\mu_0}}, \quad b_3' = \frac{b_3}{2\Omega L\sqrt{\rho_0\mu_0}},
$$

$V_{az}' = V_{az}/(LS)$, with the boundary conditions $\psi = 0$ at $y = 0,1$ where ψ denotes one of the variables (u,v,w,b_i'). For instance, we assume disturbance solutions of the form (e.g., Ref. [60]) $\psi(\boldsymbol{x},t') = \hat{\psi}(y)\exp\imath(\omega t' - k_z z)$ (axisymmetric disturbances) where ω and k_z are constant. Accordingly, the system (C1) is transformed as

$$
\begin{aligned}
&\imath\omega\hat{u} = -R_\Omega^{-2}(1+R_\Omega)\hat{v} - \imath R_\Omega^{-1}\eta\hat{b}_1,\\
&\imath\omega\hat{v} = R_\Omega\hat{u} - \frac{d\hat{p}}{dy} - R_\Omega^{-1}\left(\imath\hat{b}_2 + k_z^{-1}\frac{d\hat{b}_3}{dy}\right),\\
&\imath\omega\hat{w} = \imath k_z\hat{p} + \hat{\theta}, \quad \imath\omega\hat{b}_1 = R_\Omega^{-2}\hat{b}_3 - \imath R_\Omega^{-1}\eta\hat{u}, \quad \text{(C2)}\\
&\imath\omega\hat{b}_2 = -\imath R_\Omega^{-1}\eta\hat{v}, \quad \imath\omega\hat{b}_3 = -\imath R_\Omega^{-1}\eta\hat{w},\\
&R_\Omega^{-2}\frac{d\hat{v}}{dy} = \imath k_z\hat{w}, \quad R_\Omega^{-2}\frac{d\hat{b}_2}{dy} = \imath k_z\hat{b}_3,\\
&\imath R_\Omega^{-1}\hat{\theta} = R_i R_\Omega^{-2}\hat{b}_3 + m_0,
\end{aligned}
$$

where m_0 is a constant and $\eta = k_z V_{az}'$. From the above system, we deduce the following second differential equation for $\hat{w}(y)$:

$$
\begin{aligned}
&[(\omega R_\Omega)^4 - (2\eta^2 + R_i)(\omega R_\Omega)^2 + \eta^2(R_i+\eta^2)]\frac{d^2\hat{w}}{dy^2}\\
&\quad - \{(\omega R_\Omega)^4 - [2\eta^2 + R_\Omega(1+R_\Omega)](\omega R_\Omega)^2\\
&\quad + \eta^2(R_\Omega+\eta^2)\}\omega^2\hat{w} = 0, \qquad \text{(C3)}
\end{aligned}
$$

with solutions, subject to boundary condition $\hat{w} = 0$ on $y = 0,1$,

$$
\hat{w} = \sin(m\pi y), \quad m = 2,4,6,\ldots.
$$

The substitution of the latter solution into Eq. (C4) yields the following dispersion relation:

$$
\begin{aligned}
&(\omega R_\Omega)^4 - \left(2\eta^2 + \frac{\kappa^2}{S^2}\sin^2\alpha + R_i\cos^2\alpha\right)(\omega R_\Omega)^2\\
&\quad + \eta^2(\eta^2 + R_\Omega\sin^2\alpha + R_i\cos^2\alpha) = 0, \qquad \text{(C4)}
\end{aligned}
$$

in which $\cos\alpha = m\pi/\sqrt{m^2\pi^2 + k_z^2}$. As can be expected, the dispersion relations (37) and (C4) are similar provided $m\pi/L$ represents the radial component of the wave vector, which takes only discrete values, while its counterpart k_2 in the unbounded case varies in $]-\infty, +\infty[$.

[1] N. I. Shakura and R. A. Sunyaev, A&A **24**, 337 (1973).
[2] S. A. Balbus and J. F. Hawley, Rev. Mod. Phys. **70**, 1 (1998).
[3] P. A. Yecko, A&A **425**, 385 (2004).
[4] O. M. Umurhan, K. Menou, and O. Regev, Phys. Rev. Lett. **98**, 034501 (2007).
[5] F. Rincon, G. I. Ogilvie, and M. R. E. Proctor, Phys. Rev. Lett. **98**, 254502 (2007).
[6] G. Bodo, A. Mignone, F. Cattaneo, P. Rossi, and A. Ferrari, A&A **487**, 1 (2008).
[7] P. Goldreich and D. Lynden-Bell, Mon. Not. R. astr. Soc. **130**, 125 (1965).
[8] O. M. Umurhan and O. Regev, Mon. Not. R. Astron. Soc. **427**, 855 (2004).
[9] S. A. Balbus and J. F. Hawley, Astrophys. J. **652**, 1020 (2006).
[10] O. Regev and O. M. Umurhan, A&A **481**, 21 (2008).
[11] Rogallo, NASA Technical Memo No. 81315, 1981.
[12] G. Lesur, Ph.D. thesis, University of Grenoble I, 2007.
[13] P. Bradshaw, J. Fluid Mech. **36**, 177 (1969).
[14] D. J. Tritton, J. Fluid Mech. **241**, 503 (1992).
[15] A. Salhi and C. Cambon, J. Fluid Mech. **347**, 171 (1997).
[16] K. G. Batchelor and I. Proudman, Q. J. Mech. Appl. Math. **7**, 83 (1954).
[17] H. K. Moffatt, in *Colloquium on Atmospheric Turbulence and Radio Wave Propagation*, edited by A. M. Yaglom and V. I. Tatarsky (Nauka, Moscow, 1967), p. 139.
[18] A. A. Townsend, *The Structure of Turbulent Shear Flow* (Cambridge University Press, Cambridge, UK, New York, 1976).
[19] J. C. R. Hunt and D. J. Carruthers, J. Fluid Mech. **212**, 497 (1990).

[20] B. J. Bayly, Phys. Rev. Lett. **57**, 2160 (1986).
[21] R. T. Pierrehumbert, Phys. Rev. Lett. **57**, 2157 (1986).
[22] A. D. D. Craik, J. Fluid Mech. **198**, 275 (1989).
[23] T. Miyazaki, Phys. Fluids A **5**, 2702 (1993).
[24] C. Cambon, J.-P. Benoit, L. Shao, and L. Jacquin, J. Fluid Mech. **278**, 175 (1994).
[25] R. R. Kerswell, Annu. Rev. Fluid Mech. **34**, 83 (2002).
[26] N. R. Lebovitz and E. Zweibell, Astrophys. J. **609**, 301 (2004).
[27] A. Salhi and C. Cambon, Phys. Rev. E **81**, 026302 (2010).
[28] G. D. Chagelishvili, A. G. Tevzadze, G. Bodo, and S. S. Moiseev, Phys. Rev. Lett. **79**, 3178 (1997).
[29] A. G. Tevzadze, G. D. Chagelishvili, and J.-P. Zahn, A&A **478**, 9 (2008).
[30] P. J. Schmid, Annu. Rev. Fluid Mech. **39**, 129 (2007).
[31] S. A. Balbus, J. F. Hawley, and J. M. Stone, Astrophys. J. **467**, 76 (1996).
[32] P. Godon and M. Livio, Astrophys. J. **521**, 319 (1999).
[33] E. Knobloch, Mon. Not. R. astr. Soc. **255**, 25 (1992).
[34] Y. Shen, J. M. Stone, and T. A. Gardiner, Astrophys. J. **653**, 513 (2006).
[35] B. Dubrulle, L. Marié, C. Normand, D. Richard, F. Hersant, and J.-P. Zahn, A&A **429**, 1 (2005).
[36] A. Salhi and C. Cambon, Phys. Rev. E **81**, 026302 (2010).
[37] A. Salhi, T. Lehner, F. Godeferd, and C. Cambon (unpublished).
[38] J. Pedlowski, *Geophysical Fluid Dynamics*, 2nd ed. (Springer, Berlin, 1986).
[39] H. H. Klar, Astrophys. J. **606**, 1070 (2004).
[40] H. H. Klar and P. Bodenheimer, Astrophys. J. **582**, 869 (2003).
[41] A. G. Tevzadze, G. D. Chagelishvilli, G. Bodo, and P. Rossi, Mon. Not. Astron. Soc. **401**, 901 (2010).
[42] P. Sagaut and C. Cambon, *Homogeneous Turbulence Dynamics* (Cambridge University Press, New York, 2008).
[43] S. A. Balbus and J. F. Hawley, Astrophys. J. **376**, 214 (1991).
[44] H. P. Greenspan, *The Theory of Rotating Fluids* (Cambridge University Press, New York, 1968).
[45] S. A. Balbus and J. F. Hawley, Astrophys. J. **400**, 610 (1992).
[46] A. Salhi and C. Cambon, Phys. Fluids **19**, 055102 (2007).
[47] S. A. Balbus and J. F. Hawley, Astrophys. J. **392**, 662 (1992).
[48] J. F. Hawley, C. F. Gammie, and S. A. Balbus, Astrophys. J. **464**, 690 (1996).
[49] C. Terquem and J. C. B. Papaloizou, Mon. Not. R. Astron. Soc. **279**, 767 (1996).
[50] A. Brandenburg and B. Dintrans, A&A **450**, 437 (2006).
[51] M. S. P. Eastham, *The Asymptotic Solution of Linear Differential Systems: Applications of the Levinson Theorem* (Clarendon, Oxford, 1989).
[52] R. A. Struble, *Nonlinear Differential Equations* (McGraw-Hill, New York, 1962).
[53] J. F. Hawley, C. F. Gammie, and S. A. Balbus, Astrophys. J. **440**, 742 (1995).
[54] H. M. Blackburn, D. Barkley, and S. J. Sherwin, J. Fluid Mech. **603**, 271 (2008).
[55] H. Hanazaki and J. C. R. Hunt, J. Fluid Mech. **507**, 1 (2004).
[56] S. E. Holt, J. R. Koseff, and J. H. Ferziger, J. Fluid Mech. **237**, 499 (1992).
[57] G. D. Chagelishvili, T. S. Hristov, R. G. Chanishvili, and J. G. Lominadze, Phys. Rev. E **47**, 366 (1993).
[58] I. S. Gradshteyn and I. M. Ryzhik, *Table of Integrals, Series, and Products* (Academic, New York, 1965).
[59] A. Erdelyi, W. Magnus, F. Oberhettinger, and F. G. Tricomi, *Higher Transcendental Functions*, Vol. 1–3 (McGraw-Hill, New York, 1953).
[60] P. G. Drazin and W. H. Reid, *Hydrodynamic Stability* (Cambridge University Press, Cambridge, UK, 1981).